Acta Materialia 146 (2018) 1–16

Contents lists available at ScienceDirect

Acta Materialia

journal homepage: www.elsevier.com/locate/actamat

Full length article

# Determination of latent hardening response for FeNiCoCrMn for twin-twin interactions

S. Alkan, A. Ojha, H. Sehitoglu*

*Department of Mechanical Science and Engineering, University of Illinois at Urbana-Champaign, 1206 W. Green St., Urbana, IL 61801, USA*

ARTICLE INFO

*Article history:*
Received 27 October 2017
Received in revised form
18 December 2017
Accepted 19 December 2017
Available online 12 January 2018

*Keywords:*
High entropy alloy
Latent hardening
Twin-twin interaction
Residual dislocation
Non-Schmid twinning

ABSTRACT

Twin migration stresses and the associated latent hardening response in high entropy fcc alloys are derived corresponding to the dual interactions between all plausible twin systems. Employing an atomistically-informed, anisotropic analysis; the hardening matrix coefficients are calculated for the promising equiatomic FeNiCoCrMn high entropy alloy. The results point that the self-hardening coefficients (diagonal matrix components) are greater in magnitude than the latent hardening coefficients (off-diagonal components). This finding is a deviation from previous views in the literature which incorrectly attributed most of the hardening to latent terms. The predicted migration stresses and the strain hardening behavior exhibit a strong deviation from the Schmid law. The theoretical predictions are demonstrated to be in well agreement with the experimental trends. Furthermore, the local deviations from the stoichiometric chemical composition are shown to be of cardinal importance in the atomistic scale fault energy barrier levels.



## 1. Introduction

The high entropy alloys (HEAs) were introduced more than ten years ago [1]; however, the field took off after the demonstration of their exceptional mechanical properties [2–9]. Experimental characterization of processing-structure-property interrelationship in HEAs is ongoing while the equiatomic FeNiCoCrMn remains the most prominent HEA alloy. Despite its fame, this alloy has been mostly studied by metallurgists and developments from the mechanics side particularly to construct a framework for yielding and strain hardening are missing. This paper is an attempt to fulfill this need.

This class of alloys exhibit unusually high strain hardening coefficients [2,3,7,10] similar to twin-twin interactions in low stacking fault face centered cubic (fcc) alloys [11,12]. Twin-slip interactions are also probable to occur but the strengthening associated with twin-twin interactions are expected to dominate. In earlier works, the hardening in the primary and latent slip systems has been studied within the framework of phenomenological arguments [13–19]. The constitutive equations for flow stress evolution have been based on the following form $\dot{\tau}^{(\alpha)}_{crit} = \sum^{N}_{\alpha,\beta=1} H^{slip}_{\alpha\beta}\dot{\gamma}^{(\beta)}$ where $H^{slip}_{\alpha\beta}$ is the increase in the flow stress of the $\alpha$ system, $\dot{\tau}^{(\alpha)}_{crit}$, due to shear increment in the $\beta$ system, $\dot{\gamma}^{(\beta)}$ [20]. The hardening matrix $\left(H^{slip}_{\alpha\beta}\right)$ is composed of self-hardening $H^{slip}_{\alpha\alpha}$ (the diagonal components representing the hardening on the primary system) and the latent hardening moduli $h^{slip}_{\alpha\beta}$ (the off-diagonal terms of $\left(H^{slip}_{\alpha\beta}\right)$ with $\alpha \neq \beta$). Similar approach can be also adapted to the strain hardening in the case of twinning as being the plastic deformation mechanism (no superscript is employed in the hardening matrix for twin-twin interactions, i.e. $H^{twin}_{\alpha\beta} = H_{\alpha\beta}$). This is illustrated in Fig. 1 which highlights the corresponding critical resolved shear stress (CRSS) levels for twin nucleation and migration on a hypothetical stress-strain curve under uniaxial tension $\sigma$.

In a single pristine crystal under uniaxial loading, the activation of the primary twin system (Twin-I in Fig. 1) corresponds to the twin nucleation stress, $\tau^{N}_{crit}$. Earlier calculations indicate that $\tau^{N}_{crit}$ is governed by only the resolved shear stress acting along the primary twin system, the Schmid Factor of which is indicated as $SF_1$. Upon further deformation, the primary twin migrates at a stress level of $\tau^{T}_{crit}$ greater than $\tau^{N}_{crit}$ which is a manifestation of the self-hardening due to the twinning partials. It should be noted that $\tau^{T}_{crit}$ evolves as a function of applied strain level in connection with the increasing twinning partial density. On the other hand, it is important to distinguish that the migration of the secondary twin requires the interaction of twinning partials to increase its thickness by an additional layer unlike the twin growth and propagation

* Corresponding author.
*E-mail address:* huseyin@illinois.edu (H. Sehitoglu).

https://doi.org/10.1016/j.actamat.2017.12.058
1359-6454/

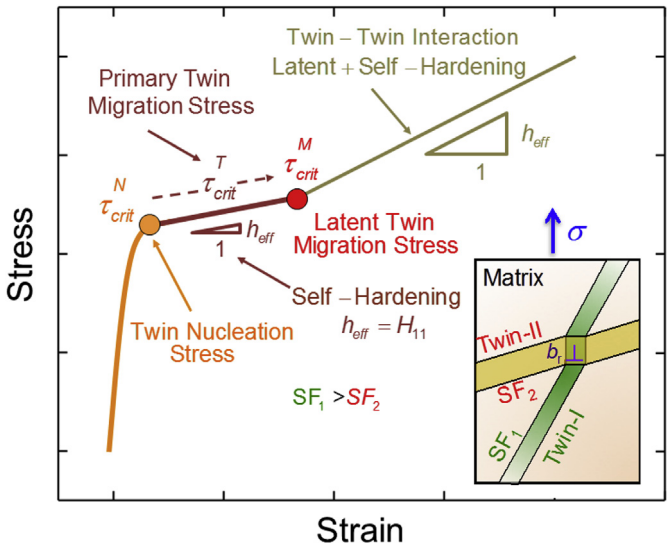


**Fig. 1.** Illustrates the critical twin nucleation stress $\tau^N_{crit}$, hardening of the primary twin migration stress, $\tau^T_{crit}$ as well as the latent twin migration stress $\tau^M_{crit}$ on a hypothetical stress-strain curve. It should be emphasized that $\tau^M_{crit}$ is greater than $\tau^T_{crit}$ in magnitude and this is reflected by the increase of strain hardening coefficient $h_{eff}$ within the twin-twin interaction regime compared to the self-hardening portion of the curve.

mechanisms discussed in the earlier literature [21–23].

The latent twin system (Twin-II in Fig. 1) is activated at a CRSS level, the ratio of which to the uniaxial stress $\sigma$ is indicated as $SF_2$ and requires a much greater stress level to migrate with twin-twin interaction, i.e. $\tau^M_{crit}$. It should be noted that $\tau^M_{crit}$ is greater than $\tau^T_{crit}$ as the energy barrier for the twinning partials gliding on the latent twin systems necessitate incorporation of the primary twinning partials on the latent twin boundary [24]. On mechanical grounds, the residual Burgers vector, $b_r$, which is an outcome of the interaction between the primary twinning dislocations and the latent twin system is believed to play a key role in the latent hardening. The effective strain hardening coefficient $h_{eff}$, which is the reflection of both self and latent hardening terms on the stress -strain curves in the case of interacting twin systems, stands out as a measure of twin migration stress evolution in response to the proceeding deformation.

The parameter of $h_{eff}$ is a function of the components of the anisotropic hardening matrix $H_{\alpha\beta}$, which depends on the quantitative analysis of mutual twin interactions. On the other hand, a rigorous derivation of $H_{\alpha\beta}$ on physical grounds stands out as a necessity since characterizing the interaction of twin systems by conventional phenomenological approaches cannot capture the corresponding defect mechanics. Furthermore, as will be discussed in the following sections, the sample-reorientation methodology followed to extract the hardening matrix coefficients from experiments in the earlier literature has significant physical limitations. Meanwhile, this operation promotes the activation of the latent system in expense of shutting off the primary system, it leads to an elevation of strengthening in favor of latent systems with an artificial loading-history effect. As a remedy, in the current work, starting with the *ab-initio* twinning energetics calculations, we outline a strategy for a predictive strain hardening model and demonstrate it for the particular case of FeNiCoCrMn HEA. The proposed model encompasses the energetics of the reactions incurring between the primary twinning partials and the latent twin boundary along with the associated crystal anisotropy. To that end, the model established on twinning dislocation energetics presents a theoretical means to determine the local stress and strain increments from the glide and the geometrical consideration of the on-going dislocation reactions at the twin-twin intersection sites. This is a major step serving as a quantitative calculation framework for different hardening matrix components (either self or latent) since pinpointing the strain and stress increments on the interacting systems is a strenuous task pointed out in the earlier literature [25,26]. The results suggest the key role played by the vector $b_r$ and the generalized planar fault energy curve (GPFE or $\gamma-$curve) on the twin migration. Therefore, the model lays out a micromechanical foundation to pinpoint the twin migration stress levels with a bottom-up approach. The resulting predictions are adopted to the single and polycrystalline configurations in FeNiCoCrMn alloys and shown to yield close agreement with the experimental measurements.

As we mention above, the current study takes a novel approach, and in our opinion the correct one, for the evaluation of self and latent hardening coefficients building upon the key earlier literature [15,19,25,27]. As a major distinction, it has been common to establish the latent hardening coefficients by shutting off the primary system and activating the latent system (by reorienting the sample). On the other hand, in reality, the primary system always remains active and must factor in the evaluation of primary (self)/latent coefficients over the course of the deformation. To that end, reorientation of the sample introduces an artificial loading-history effect which does not exist for monotonic experiments. Furthermore, the present work scrutinizes the key role of the residual Burger's vector introduced at the intersection site of primary and latent systems which is demonstrated to be responsible for the considerable elevation in the primary hardening. The presence of the residual dislocation underlies the promoted hardening along primary system in contrast to the assumptions of previous works. To that end, the present paper allows for an accurate determination of the anisotropic hardening coefficients in tune with experiments. Furthermore, apart from predicting the response of FeNiCoCrMn which undergoes twinning as the main plastic flow mechanism at 77 K, the present work also represents a major advance in the field of primary/latent hardening for twinning materials by correctly appropriating the primary/latent hardening coefficients.

Although the fcc structured, solutionized single phase FeNiCoCrMn leads to the conception of a prevailing disorder in the long-range, this does not restrain the formation of possible short-range departures from the randomness in the atomic configuration. The proposed anisotropic model accounts for the short-range ordering effects which are demonstrated to prevail on the fault energetics in FeNiCoCrMn HEA. Among the five constituent elements, Co concentration on the active twin system is shown to be of major importance in the twin nucleation and migration energetics. This composition effect acts in a fashion similar to Suzuki segregation mechanism [28] and governs also on the hardening behavior through the corresponding energy terms. On the other hand, no comprehensive and quantitative analysis has been provided on this short-range order effect present in the earlier literature on HEAs. To that end, in this work, its contribution on the twin migration and hardening phenomena will be elaborated in a detailed fashion.

We have organized the paper as follows: in section (2), we discuss the fundamentals of twin migration. In section (3), we highlight the atomistic procedures, and establish the material parameters involved in the corresponding energy barrier calculations employed for pinpointing the migration stress levels. In section (4), we proposed a crystal plasticity based criterion to construct the self and latent hardening matrices for the single and polycrystalline samples. Discussion of the results on physical and mechanistic grounds are provided in section (5). Furthermore, three appendices are included in order to supplement the quantitative analyses presented. Finally, the conclusions drawn are summarized in

section (6).

## 2. The nomenclature for twinning

In Table 1, the 12 possible twin systems (designated in Roman numerals) in fcc crystals are designated by employing a different color coding for each distinct system. The nucleation of the twins are governed by the resolved stress level of $\tau^{N}_{crit}$ acting along the twinning systems. Following the formation of the primary and latent twins, as the deformation proceeds, these twin systems interact and the twin migration stresses $\tau^{T}_{crit}$ and $\tau^{M}_{crit}$ are modified for continued plastic flow. While twin nucleation and migration have been addressed in previous works [24,29,30], the twin-twin interaction, and the subsequent latent hardening effects need further quantification.

On mechanical grounds, both self and latent hardening phenomena are manifested through the energetics of the twinning partials' glide and the on-going dislocation reactions at the intersection sites of the crossing twins. To that end, accurate determination of the residual Burgers vectors, $b_r$, along with the corresponding atomistic scale energy barriers is of paramount importance in building a comprehensive understanding for the twin-twin interactions and the resulting hardening phenomenon. In order to accomplish this task, a multiscale (continuum-atomistic) model has been established in the following section.

## 3. Modelling of the twin migration stress

### 3.1. Ab-initio density functional theory calculations

A commercially available software, Vienna Ab-initio Simulations Package (VASP) was used to perform the ab-initio calculations. The ground energy calculations were based on the generalized gradient approximation using the projector augmented wave method [31,32]. A $9 \times 9 \times 9$ $k$-point resolution was employed for the Brillouin zone integration via Monkhorst Pack method [33]. The chosen $k$-point resolution was determined based on the converged energy values which are verified by the independent test simulations. Spin polarization is also incorporated into the calculations to account for the paramagnetism in FeNiCoCrMn alloy. In the current work, a saturation magnetization of 286 emu/cc is employed. The simulations were conducted with a force cut-off corresponding to $5x10^{-3}\ eV/A^{o}$. The plane wave basis set was employed with the energy cut off specified as 500 eV. The lattice constant of fcc FeNiCoCrMn, $a$, was determined as 3.60 Å, which is close to the experimental value of 3.61 Å [6] as can be seen in Table 2.

To generate the GPFE curve along the {111}<112> twinning sense, we delineated a simulation box consisting of 13 layers oriented along the $\left(\bar{1}\,\bar{1}\,\bar{1}\right) - \left(\bar{2}11\right) - \left(01\bar{1}\right)$ direction axes in cubic coordinate frame. The number of layers are determined based on the minimum box size observed to be sufficient to obtain the converged values in the preliminary calculations. Even though FeNiCoCrMn has of disordered fcc structure, we meticulously consider the positions of the atoms of the five constituent elements on an iterative basis, as the concentration increase in Co atoms close to the fault is evaluated to minimize the energy values significantly. In the minimum energy configuration, the concentration of Co atoms are determined to gradually decrease furthering away from the fault plane following the concentration function $C(x)$: $(3x^2\text{-}28x{+}69)\%$ (the units of x is in Å) as shown in Fig. 2(a). On the other hand, the variation of energy in response to the concentration change of the other solute elements along the fault planes do not exceed 8% even in the second highest case of Mn after Co. Therefore, throughout the fault energetics analysis provided in this work, only the change of Co concentration is focused.

Following our earlier works on simulation methodologies [24,29], we undertake relaxation schemes parallel to the twin fault to obtain the accurate GPFE parameters as depicted in Fig. 2(b). In order to generate the GPFE curve illustrated in Fig. 2 (b), the atomic layers normal to the [111] direction are sheared with an amount of disregistry, $u_x$, consecutively. In Fig. 2(b), $\gamma$ energy vs $u_x$ is plotted employing a normalization factor $b$, i.e. $b = |a/6 < 112 >|$, which corresponds to the magnitude of a twining partial in fcc lattice. It should be noted that the variation of $u_x/b$ within the [0,1], [1,2] and [2,3] intervals corresponds to the shearing along first, second and third atomic layers respectively. Meanwhile the shearing of the first layer has to overcome an energy barrier of $\gamma_{us}$- unstable stacking fault energy, the following shearing layers encounter with an energy barrier level of $\gamma_{ut}$- unstable twin stacking fault energy. It is to be noted that after the third layer, $\gamma_{ut}$ level saturates which corresponds to a three-layered stable twin nucleus geometry.

In the present work, for the minimum energy configuration with Co concentration of 69% regarding the $C(x)$ function, the $\gamma_{us}$ and -intrinsic stacking fault energy$\gamma_{isf}$, values along the {111} <112> twin system are evaluated to be as 439 $mJm^{-2}$ and 8 $mJm^{-2}$ respectively. On the other hand, for lower Co concentrations of 40% and 20%, the $\gamma_{isf}$ levels corresponds to 22 $mJm^{-2}$ and 43 $mJm^{-2}$. A similar trend has also been observed to govern on the $\gamma_{us}$ and $\gamma_{ut}$ levels. For example, for local Co concentration levels of 20% and 40%, the energy barriers of $\gamma_{us}$ and $\gamma_{ut}$ correspond to the sets of {516, 493} and {609, 584} respectively in units of $mJ/m^2$. As these values suggest, the increasing local Co atom concentration diminishes the energy barrier levels in FeNiCoCrMn HEA. To that end, the minimum energy configuration of $\gamma_{isf}$ governed by $C(x)$ is employed throughout the following analysis. Similarly, the elastic modulus of the {111}<112> twin system is calculated as 55 GPa by taking the maximum slope of the $\gamma$ curve, i.e.$\mu_{\{111\}<112>} = \max\left(2\pi \frac{\partial \gamma}{\partial u_x}\right)$[34–36]. Adopting the twin nucleation formulation developed in our previous works [37,38] which is detailed in Appendix A, $\tau^{N}_{crit}$ is calculated as 170 MPa which is in excellent agreement with the experimental value of 168 MPa as

**Table 1**
Possible twin systems in an fcc crystal (as illustrated in Fig. B1 employing Thompson tetrahedron).

| Twin systems | | | | |
|---|---|---|---|---|
| | I | II | III | IV |
| | $(11\bar{1})[\bar{1}\bar{1}2]$ | $(1\bar{1}1)[1\bar{1}\bar{2}]$ | $(\bar{1}11)[\bar{1}\bar{1}2]$ | $(1\bar{1}1)[12\bar{1}]$ |
| | V | VI | VII | VIII |
| | $(\bar{1}\bar{1}1)[\bar{1}2\bar{1}]$ | $(111)[1\bar{2}\bar{1}]$ | $(\bar{1}11)[\bar{1}\bar{2}1]$ | $(\bar{1}11)[21\bar{1}]$ |
| | IX | X | XI | XII |
| | $(\bar{1}\bar{1}1)[2\bar{1}\bar{1}]$ | $(1\bar{1}1)[\bar{2}\bar{1}1]$ | $(111)[\bar{2}11]$ | $(111)[11\bar{2}]$ |

**Table 2**
The GPFE parameters, shear modulus $\mu_{\{111\}<112>}$, the twinning dislocation Burgers vector magnitude ($b$), the {111} interplanar distance ($d_{\{111\}}$) and the twinning shear ($s$) along with the $\tau^N_{crit}$ levels predicted from the theoretical calculations and measured in the experiments are tabulated for the equiatomic FeNiCoCrMn alloy.

| $\gamma_{us}$ (mJm$^{-2}$) | $\gamma_{isf}$ (mJm$^{-2}$) | $\gamma_{ut}$ (mJm$^{-2}$) | $2\gamma_{tsf}$ (mJm$^{-2}$) | $\mu_{\{111\}<112>}$ (GPa) |
|---|---|---|---|---|
| 439 | 8 | 538 | 14 | 55 |
| Burgers vector $b$ (Å) | $d_{\{111\}}$ (Å) | Twinning shear ($s$) | $\tau^N_{crit}$ (MPa) Theory (This study) | $\tau^N_{crit}$(MPa) Experiment |
| 1.47 | 2.07 | 0.71 | 170 | 168 |

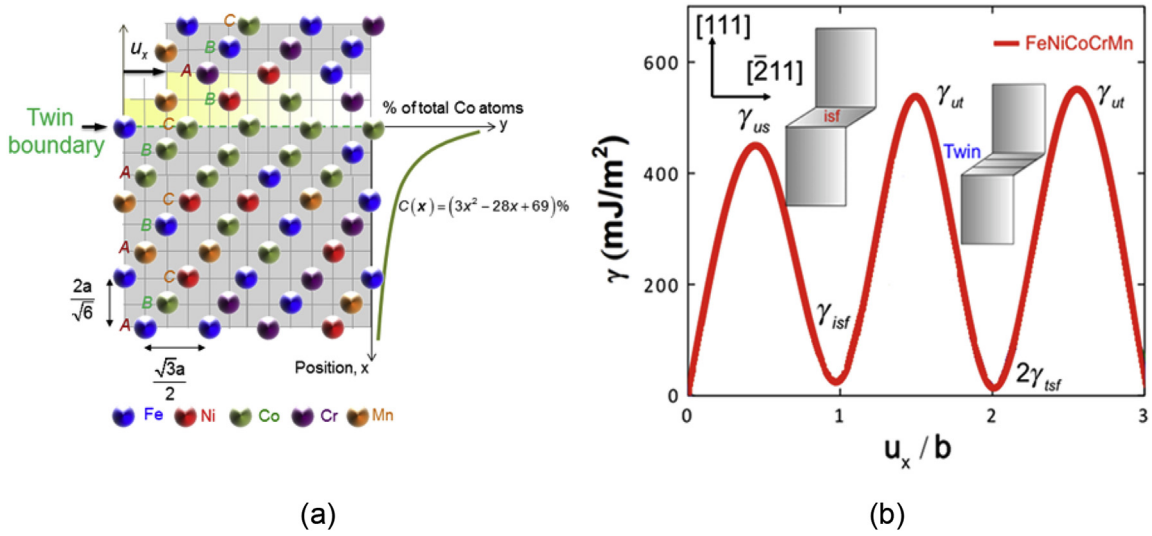


**Fig. 2.** (a) Distribution of Co atoms that leads to the minimum intrinsic stacking fault energy, $\gamma_{isf}$. (b) The GPFE curve for FeNiCoCrMn is plotted. In the plot, the extrema points of $\gamma_{us}$ $\gamma_{ut}$, $\gamma_{tsf}$ correspond to the unstable stacking fault, unstable twin stacking fault and twin stacking fault energy levels respectively.

tabulated in Table 2 [4]. The rather low value of the stacking fault energy in FeNiCoCrMn HEA is distinguishing and plays a key role in the conducive nature of the alloy to twinning.

### 3.2. Formulation of the twin migration stress

In this section, the resolved shear stress values corresponding to the migration of the interacting primary and latent twin systems, $\tau^T_{crit}$ and $\tau^M_{crit}$, are calculated based on the minimization of the total energy, $E_{total}$, which corresponds to the configuration shown in Fig. 3. In this geometry, the primary and the latent twins intersect along the line $\zeta_1$, and a residual Burgers vector $b_r$ is left behind following the interaction of the latent twin boundary with the incident partials. It is to be noted that the twinning dislocation, $b_2$, which migrates the boundary of the latent twin follows an energy path-way dependent on $b_r$ as previously discussed by Sehitoglu et al. [24,39–41]. This modification is inextricably linked with the local stress field introduced by $b_r$. Considering that $b_r$ is a function of the interaction geometry and therefore loading orientation, the expression for $E_{total}$ depicting the twinning energetics exhibits strong anisotropy as will be further interrogated in the following sections.

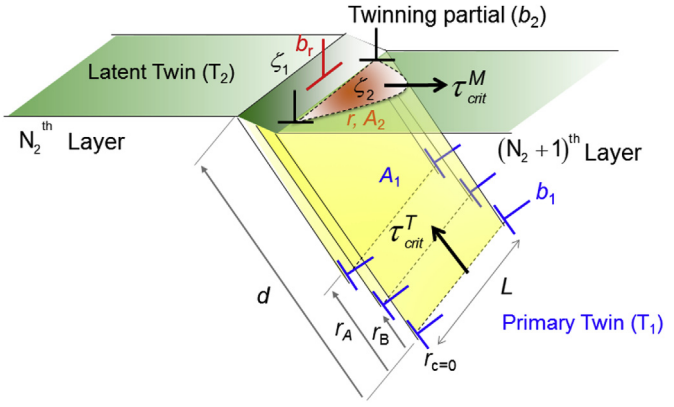


**Fig. 3.** Schematic of a twin-twin interaction considered in the present analysis. The incident twin (T1) is the primary twin and the secondary twin (T2) is the latent twin. It is to be noted that the primary twinning dislocations, $b_1$, interact with the latent twin boundary and form the residual Burger's vector $b_r$ as well as the twinning partial $b_2$ which migrates the latent twin boundary.

On mathematical grounds, the $E_{total}$ expression describing the twin-twin interaction comprises the following: (i) the line energies of the twinning dislocations, including the primary $E_{primary}$, and, the latent $E_{latent}$, twinning partials as well as of the residual dislocation $b_r$, i.e. $E_{residual}$ , (ii) the elastic dislocation-dislocation interaction energy $E_{interaction}$, (iii) dislocation-solute interaction energy, $E_{D-S}$, (iv) the misfit energy of the primary twin, $E_{incidentGPFE}$, (v) the modified misfit energy of the latent twin, $E_{modifiedGPFE}$, (vi) the external work done to move the incoming and migrating twinning dislocations, i.e. $W_{primary}$ and $W_{latent}$ respectively. In summary, the following equation incorporating the anisotropy of the crystal can be postulated for the total energy, $E_{total}$:

$$\begin{aligned} E_{total} &= E_{primary} + E_{latent} + E_{residual} + E_{\text{interaction}} + E_{D-S} + E_{incidentGPFE} + E_{modifiedGPFE} - W_{primary} - W_{latent} \\ &= \frac{Kb_1{}^2}{4\pi}\ln\left(\frac{R}{\xi}\right)(2d+\zeta_1) + \frac{Kb_2^2}{4\pi}\ln\left(\frac{R}{\xi}\right)(l_2-\zeta_2) + \frac{Kb_r^2}{2\pi}\ln\left(\frac{R}{\xi}\right)\zeta_2 \\ &\quad -\frac{K}{2\pi}\left(b_1b_r\ln\left(\frac{r_B-r_A}{r_o}\right) + b_1b_2\ln\left(\frac{r_B}{2r_o}\right) + b_2b_r\ln\left(\frac{r_A}{r_o}\right)\right)\zeta_1 \\ &- \int C(x)\sigma_{ij}^{disl}\varepsilon_{ij}^{*}dV + \sum_{m=1}^{N_1}\gamma_{incidentGPFE}a' + \sum_{m=N_2}^{N_2+1}\gamma_{modifiedGPFE}a' - \tau_{crit}^{T}b_1A_1 - \tau_{crit}^{M}b_2A_2 \end{aligned} \tag{1}$$

In Eq. (1), $A_1$ and $A_2$ are the areas swept by the incident and outgoing twinning partials on the verge of twin migration and can be written as $A_1 = (d - r_A)L$ and $A_2 = \frac{\pi}{8}(\zeta_2)^2$ respectively. Similarly, the term $l_2$ is equal to $\frac{\pi}{2}\zeta_2$ and the differential $dV$ can be written as $\pi r^2 d\zeta_2$ where $r$ is the radial coordinate vector varying from 0 to 2 times {111} inter-planar spacing, i.e. $2d_{\{111\}}$.The outer core $R$ can be approximated as $500\xi$ for the dislocations involved in the calculations, where $\xi$ is the half core-width of the dislocation taken as equal to half inter-planar spacing $0.5d_{\{111\}}$.

As can be seen in Eq. (1), the expression for $E_{total}$ incorporates the atomistic scale GPFE information into the dislocation-based mechanistic formulation without any *a priori* empirical constants. The detailed discussion on the determination of the twinning partial separation distances $d_1 = r_A - r_B$ and $d_2 = r_B - r_C$ are discussed in Appendix A. The terms $N_1$ and $N_2$ are the corresponding layers of the primary and latent twins. Among the atomistic scale parameters involved, the term $\gamma_{\text{modifiedGPFE}}$ corresponds to the modified misfit energy to be overcome by the migration of the twinning dislocation $b_2$ after $b_r$ is left at the twin boundary. Following the methodology presented in our earlier work [24], $\gamma_{\text{modifiedGPFE}}$ is generated in Appendix A.

The *ab-initio* calculations suggest that the formation of intrinsic and extrinsic stacking faults in Co rich planes are energy-wise more favorable as shown in Fig. 2. The presence of a short-range composition gradient $C(x)$ introduces an interaction energy between the partials and the Co solute atoms which can be characterized by the stress field of the partial dislocation $\sigma_{ij}^{disl}$ and $\varepsilon_{ij}^{*}$, i.e. the misfit strain introduced by the Co solute atoms with respect to the elastic matrix [42]. The tensor $[\varepsilon_{ij}^{*}]$, is of hydrostatic character and its diagonal terms are evaluated to be equal to −0.016 based on the volumetric contraction of the FeNiCoCrMn alloy $_o$lattice ($a$=3.60$\AA$) with respect to the local lattice parameter of 3.54$\AA$ at the high concentration Co zones. Thus, the components of $\varepsilon_{ij}^{*}$ are given as follows:

$$\varepsilon_{ij}^{*} = -0.016\delta_{ij} \tag{2}$$

On the other hand, the anisotropic stress field of $\sigma_{ij}^{disl}$ is expressed in the orthonormal dislocation frame parallel to the $\left(01\bar{1}\right) - \left(\bar{1}\,\bar{1}\,\bar{1}\right) - \left(\bar{2}11\right)$ vector triad as [42,43]:

$$\left(\sigma_{ij}^{disl}\right) = \frac{Kb}{2\pi r}\begin{pmatrix} -\sin\psi\left(1+2\cos^2\psi\right) & \cos\psi\cos2\psi & 0 \\ \cos\psi\cos2\psi & \sin\psi\cos2\psi & 1 \\ 0 & 1 & -\sin\psi \end{pmatrix} \tag{3}$$

where $K$ is an anisotropic coefficient as evaluated in Appendix A. r and $\psi$ are the position vector and the angle between the position vector and the glide direction respectively.

Following the determination of the long-range and short-range energy terms in Eq. (1), the migration stress for the latent twin system, $\tau_{crit}^{M}$, can be calculated by minimization of the $E_{total}$ expression with respect to the parameter of as follows [24]:

$$\frac{\partial E_{total}}{\partial \zeta_2} = 0 \tag{4}$$

The expression in Eq. (4) along with the explicit $E_{total}$ formulation, leads to $\tau_{crit}^{M}$ as follows:

$$\tau_{crit}^{M} = \frac{\sum_{m=N_2}^{N_2+1}\gamma_{\text{modifiedGPFE}}a' + \frac{Kb_2^2}{2\pi}\ln\left(\frac{R}{\xi}\right)(l_2-\zeta_2) - \int C(x)\varepsilon_{ij}^{*}dV}{\frac{Kb_2b_r}{2\pi}\ln\left(\frac{R}{\xi}\right) + \frac{Kb_2^2}{4\pi}\ln\left(\frac{R}{\xi}\right)(l_2-\zeta_2)} \tag{5}$$

Eq. (5) clearly shows that $\tau_{crit}^{M}$ depends on $b_r$, the self and interaction energies of the twinning partials and the modified misfit energy values as well as the dislocation-solute interaction. Similarly, the twinning stress for the primary system $\tau_{crit}^{T}$ can be calculated from the $E_{total}$ expression by minimization with respect to $\zeta_1$ [24], which is expressed as:

$$\frac{\partial E_{total}}{\partial \zeta_1} = 0 \tag{6}$$

Explicit calculation of Eq. (6) results in the following expression for the twinning stress of the primary system, $\tau_{crit}^{T}$ :

$$\begin{aligned} \tau_{crit}^{T} = \frac{1}{b_1r_A}\Bigg\{ &-\frac{Kb_1{}^2}{2\pi}\left(\ln\left(\frac{r_B-r_A}{2r_o}\right) + \ln\left(\frac{r_B}{r_o}\right) + \ln\left(\frac{r_A}{r_o}\right)\right) \\ &-\frac{Kb_1b_r}{2\pi}\ln\left(\frac{r_A}{2r_o}\right)\Bigg\} + \frac{1}{b_1}\sum_{m=1}^{N_1}\gamma_{incidentGPFE}a' \\ &- \int C(x)\sigma_{ij}^{disl}\varepsilon_{ij}^{*}dV \end{aligned} \tag{7}$$

The ratio of $\tau_{crit}^{M}/\tau_{crit}^{N}$ for different single crystal orientations under uniaxial tension and compression are provided in Table 3 and Fig. 4. The sample orientations are selected based on the available experimental data on FeNiCoCrMn conducive to twinning which are <111>, <122>, <123> and <144> tension and <010> compression cases (from the experiments conducted by our group [4] at room temperature and 77 K) along with the <111> and <149> tension results by Kireeva et al. [44,45]. Twinning in the other orientations are unlikely except at very high stresses because of their low *SF* values. The tabulated data suggest that $\tau_{crit}^{M}/\tau_{crit}^{N}$ ratio increases as $b_r$ becomes greater (a detailed derivation for $\tau_{crit}^{N}$ is provided in Appendix A). The modified GPFE, $\gamma_{\text{modifiedGPFE}}$, in the presence of a non-zero $b_r$, exhibits a higher energy barrier for twin migration compared to the case when $b_r = 0$ as detailed in

**Table 3**
Summarizes the active twin systems in tension (T) and compression (C) along with the Schmid Factors (*SF*) as well as the variation of the ratio of the twin-migration stress ($\tau^{M}_{crit}$) for the latent system to the twin nucleation stress ($\tau^{N}_{crit}$) as a function of $b_r$ for the interacting {111}<112> twin systems.

| | Orientation | Incoming Twin (T1) | SF T1 | Outgoing Twin (T2) | SF T2 | Residual dislocation ($b_r$) | $\frac{\tau^{M}_{crit}}{\tau^{N}_{crit}}$ |
|---|---|---|---|---|---|---|---|
| T | <122> | VIII | 0.47 | XI | 0.26 | 0.59a | 1.12 |
| | <111> | IV | 0.32 | VIII | 0.32 | 0.70a | 1.20 |
| | <144> | VIII | 0.50 | XI | 0.38 | 0.70a | 1.20 |
| | <123> | VIII | 0.47 | IV | 0.26 | 0.82a | 1.35 |
| C | <144> | VII | 0.25 | III | 0.25 | 0.70a | 1.20 |
| | <010> | VI | 0.47 | VII | 0.47 | 0.82a | 1.35 |
| | <123> | III | 0.33 | XII | 0.30 | 1.22a | 1.61 |

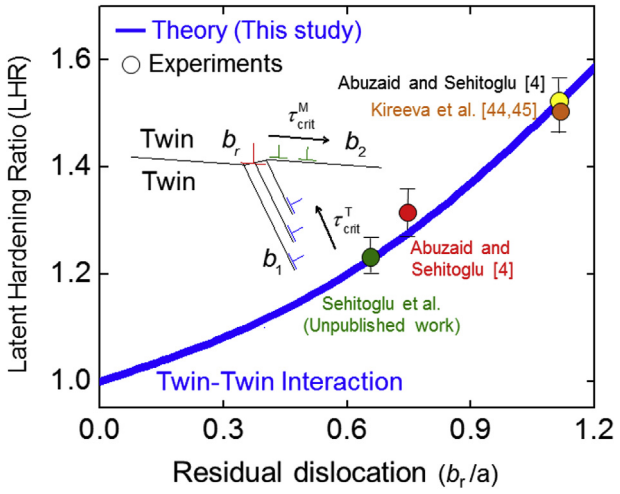


**Fig. 4.** The latent hardening ratio (LHR), i.e. $\tau^{M}_{crit}/\tau^{N}_{crit}$, is plotted as a function of the residual dislocation $b_r$ in FeNiCoCrMn high entropy alloy. For comparison purposes, the experimental values are taken from references [4,44,45] and our unpublished work.

Appendix B and also confirmed by the previous studies incorporating twinning dislocation reactions [24,29]. This modification promotes the resistance exerted by the interatomic forces against the disregistry shearing and thereby introduces an hardening effect on $.\tau^{M}_{crit}$

The promotion of the hardening ratio $\tau^{M}_{crit}/\tau^{N}_{crit}$ in the experiments with $b_r$ [4,44,45] complies with the theoretical findings of this study and underpins the significance of the local interaction between the twinning partials. The resulting values suggest that the twinning-induced latent hardening in FeNiCoCrMn HEA plays a significant role and hence a theoretical model encompassing the contribution of the crossing -twins on the hardening levels should be developed. In the following section, this task is accomplished by nurturing the crystal plasticity flow rule formulation [20,46] with the twin migration analysis herein introduced.

## 4. Determination of latent hardening

### 4.1. Formulation of latent hardening model

The twin migration calculations developed so far consider a geometry composed of only two interacting twins. On the other hand, the experimental evidence suggests that the number of interacting twins can be greater than 2. In order to elaborate on the latent hardening effects for the scenarios where multiple twin-twin interaction combinations incur, we employed a linear discrete relationship between the increment of the migration stress corresponding to the $\alpha^{\text{th}}$ twin system $\dot{\tau}^{M(\alpha)}_{crit}$ in response to the shearing on the $\beta^{th}$ twin system $\dot{\gamma}^{(\beta)}$ as follows:

$$\dot{\tau}^{M(\alpha)}_{crit} = \sum_{\alpha,\beta=1}^{12} H_{\alpha\beta}\dot{\gamma}^{(\beta)} \tag{8}$$

In the expression of Eq. (8), the $H_{\alpha\beta}$ is the hardening modulus which is evaluated based on the anisotropic, multiscale twin migration model introduced in Section 3 and Appendix B. It is to be noted that this formulation is a particular form of the differential hardening rate equation initially proposed by Hill [20] adapted to the monotonic loading geometry. In the formulation employed, both $\dot{\tau}^{M(\alpha)}_{crit}$ and $\dot{\gamma}^{(\beta)}$ components are described with respect to a local crystal coordinate frame convecting with the lattice itself. On the other hand, no elastic strain component is involved in the calculations as we mainly focus on a stage of plastic regime at which the plastic strains originating from the primary and latent twin nucleation phenomena are exceedingly higher than the elastic strain.

### 4.2. Hardening matrices for single crystals

In this section, we adopted the hardening formulation, Eq. (8), for a number of uniaxial tension/compression orientations and compare the theoretical estimations for the $H_{\alpha\beta}$ values along with the experimental measurements as can be seen in Table 4. To accomplish this task, we focused on the <010> compression and the <123>, <122> and <111> tension orientations. As can be seen in Table 4, the hardening slope, $h_{eff}$, exhibits crystallographic anisotropy linked with the components of $H_{\alpha\beta}$. The results suggest that the greatest hardening is observed along the <111> loading direction among the single crystalline tension samples which have the same number of active twin systems with the others. Considering the fact that the values of $b_r$ as tabulated in Table B1 are similar for these three tension samples analyzed, the *SF* differentials of the active twin systems are expected to contribute to the distinct hardening slope values. On experimental grounds, the close *SF* values for the active systems under uniaxial loading increases the frequency of twin-twin interactions and therefore contributes

**Table 4**
The hardening matrix, $H_{\alpha\beta}$ in GPa units for different orientations in tension and compression are tabulated. The values obtained experimentally are provided for comparison.

| Orientations | Number of twin systems active | Hardening matrix, $H_{\alpha\beta}$ (GPa)(This study) | Hardening Slope, $h_{eff}$ (GPa) (Theory-This study) | Experimental hardening slope, $h_{eff}$ (GPa) |
|---|---|---|---|---|
| <111> (T) | 3 | $\begin{bmatrix} 1.4 & 0.45 & 0.45 \\ 0.45 & 1.4 & 0.45 \\ 0.45 & 0.45 & 1.4 \end{bmatrix}$ | 1.82 | 1.7–2 [44]<br>1.8 (unpublished work-Sehitoglu) |
| <123> (T) | 3 | $\begin{bmatrix} 1.1 & 0.34 & 0.34 \\ 0.34 & 1.1 & 0.34 \\ 0.34 & 0.34 & 1.1 \end{bmatrix}$ | 1.46 | 1.4 [4] |
| <122> (T) | 3 | $\begin{bmatrix} 1.1 & 0.34 & 0.34 \\ 0.34 & 1.1 & 0.34 \\ 0.34 & 0.34 & 1.1 \end{bmatrix}$ | 1.46 | 1.4 [4] |
| <010> (C) | 4 | $\begin{bmatrix} 2.4 & 0.93 & 0.93 & 0.45 \\ 0.93 & 2.4 & 0.93 & 0.45 \\ 0.93 & 0.93 & 1.4 & 0.45 \\ 0.45 & 0.45 & 0.45 & 1.4 \end{bmatrix}$ | 2.71 | 2.60 (Unpublished work-Sehitoglu) |
| Polycrystal (T) | Multiple | - | 3.09 | 1.5–3.5 [2,3] |

to the internal stress promoting higher resultant $h_{eff}$ values. Similar latent hardening behavior has been also observed in slip-induced hardening of pure Al and Cu as a result of pronounced dislocation density in orientations of multiple slip with close *SF*'s [16].

The hardening slope of <010> orientation under uniaxial compression is significantly higher as a result of more number of active twin systems, i.e. 4 instead of 3, and the prominent non-Schmid asymmetry effects involved in $\tau^{M}_{crit}$ levels as illustrated in Appendix C in a detailed fashion. Moreover, it is to be noted close values of *SF*'s contribute to the promotion of $h_{eff}$ value for <010> compression similar to the tension orientations. To that end, $h_{eff}$ for single crystals under uniaxial loading is deduced to be governed by both anisotropic $\tau^{M}_{crit}$ values as well as the *SF* differential between the interacting twin systems.

### 4.3. Hardening matrices for polycrystals

In this section, the hardening formulation is further extended to the polycrystalline FeNiCoCrMn HEA. In order to accomplish this task, $5 \times 5 \times 5$ (=125) grains were created via changing the Euler angles such that the misorientation between two adjacent crystals do not exceed 10°. For kth grain considered, i.e. $1 \leq k \leq 125$, the increment of the plastic work, $dW_{plastic}$ per unit volume is given as:

$$dW_{plastic} = \tau_k^{(\alpha)} \sum_{\alpha=1}^{12} \dot{\gamma}_k^{(\alpha)} \tag{9}$$

In Eq. (10), the flow stress on the $\alpha^{\text{th}}$ twin system, i.e. $\tau_k^{(\alpha)}$equal to CRSS for the $\alpha^{\text{th}}$ system, is expressed on mathematical grounds as:

$$\tau_k^{(\alpha)} = \sum_{k=1}^{12} \left( H_{\alpha\beta}^{k} \dot{\gamma}_k^{(\alpha)} \right) \tag{10}$$

where the shear strain increment on the $\dot{\gamma}_k^{(\alpha)}$ can be expressed as the multiplication of the crystallographic twinning shear $\gamma^{twin}$, i.e. 0.70 for an fcc structure, and $\dot{f}_k$ which is the volume fraction increment of the k$^{\text{th}}$ twin expressed as:

$$\dot{\gamma}_k^{(\alpha)} = \dot{f}_k \, \gamma^{twin} \tag{11}$$

We note that in the description of Eq. (11), the contribution from slip, i.e. equal to $(1 - f_k)\dot{\gamma}^{slip}$, to the overall shear strain rate is considered to be of minor effect as the corresponding $b_r$ values in slip-slip and slip-twin interactions are smaller than the ones involved in the twin-twin interactions [23,47–49]. This is noted in the experiments and will not change the results in our formulation. Furthermore, the total shearing taking place in each k$^{\text{th}}$ grain is evaluated based on:

$$d\tilde{\gamma}_k = \sqrt{\sum_{\alpha=1}^{12} \dot{\gamma}_k^{(\alpha)} \mathbf{M}^{(\alpha)} : \dot{\gamma}_k^{(\alpha)} \mathbf{M}^{(\alpha)}} \tag{12}$$

where the $\mathbf{M}^{(\alpha)}$ tensor is evaluated as the symmetric part of the outer product of the normalized twin plane normal, $\mathbf{n}^{(\alpha)}$ , and direction, $\mathbf{m}^{(\alpha)}$, vectors of the $\alpha^{\text{th}}$ twin system:

$$\mathbf{M}^{(\alpha)} = \frac{1}{2} \left( \mathbf{n}^{(\alpha)} \otimes \mathbf{m}^{(\alpha)} + \mathbf{m}^{(\alpha)} \otimes \mathbf{n}^{(\alpha)} \right) \tag{13}$$

It should be noted that the parameter $d\tilde{\gamma}_k$ inside the k$^{\text{th}}$ grain is analogous to the effective strain measure of the classical von-Mises theory [50]. The shear increments are known for each system based on the Burgers vector (including the residuals) and lattice spacing, which depend on the orientation of the individual grain orientation. Hence, the constraint effect, i.e. Taylor, Sachs or self-consistent, does not enter the equation because strain range at the grain level are specified from the atomistically-informed geometrical considerations [46]. The effective flow stress $\tilde{\tau}$ is calculated based on the conservation of the plastic work done on the system as:

$$dW_{plastic} = \tilde{\tau} d\tilde{\gamma} = \sum_{k=1}^{125} \sum_{\alpha=1}^{12} \tau_k^{(\alpha)} : d\gamma_k^{(\alpha)} \tag{14}$$

Following the determination of $d\tilde{\tau}$, the effective hardening modulus, $h_{eff}$, is calculated as:

$$h_{eff} = \frac{d\tilde{\tau}}{d\tilde{\gamma}} \tag{15}$$

In our first set of simulations, it is assumed that the deformation is sufficiently high to render all 125 grains plastic with internal twinning. We calculated the effective hardening modulus ($h_{eff}$) in the current work for a polycrystal to be 3.09 GPa (Table 4) using two most plausible twin systems per grain first. Then, we checked the activation of up to three activated twin systems per grain which changes the interaction matrix (as shown in Appendix B) but the

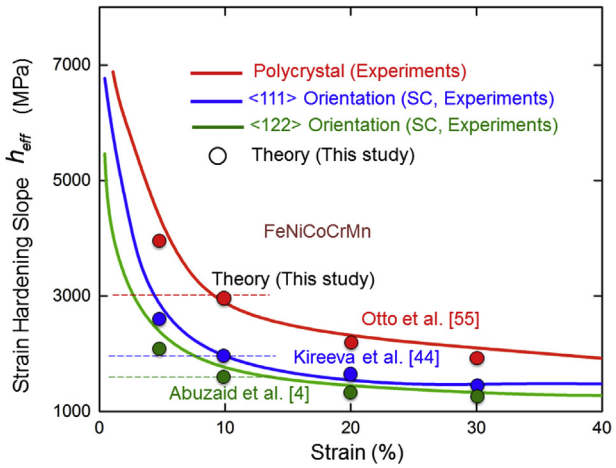


**Fig. 5.** Experimental strain hardening curves are plotted as a function of the total strain for the polycrystalline and single crystal (SC) FeNiCoCrMn HEA in comparison with the reported results in the literature [4,44,55].

effect on the results is less than 5% ($h_{eff}$ = 3.15 GPa).

The possibility of grains that remain elastic could influence the results, but since we consider strain levels far exceeding 10%, the assumption of multiple twin systems being operative (no elastic grains) in the polycrystalline case has virtually no effect on the results. This entails that the strain hardening modulus is a reflection of the twin dislocation approaching the latent twin boundary and upon its incorporation to migrate the secondary twin partials. On the other hand, the prediction of the complete stress-strain curve requires to incorporate the twin volume fraction into the analysis as the total shear strain is directly linked with the weighted contribution of the twinning shear [51,52]. At this stage an analogy can be established with the tangent moduli of self-consistent methods [53,54] employed in modelling efforts of the slip mediated plasticity such that an initial strain state information is necessary to assure the integration of stress vs strain curve on mathematical grounds reflecting the strain history.

In Fig. 5, we plot the strain hardening parameter $h_{eff}$, obtained from the experimental work (by our group [4] as well as references [44,55]) as a function of the total strain for both single and polycrystal FeNiCoCrMn HEA. The theoretical results obtained in the current study are also plotted therein for comparison purposes at 5%, 10%, 20% and 30% strain levels meanwhile it is important to note that the strain hardening is initially higher at smaller strains and decreases with further straining. It is observed that the strain hardening parameter for a polycrystalline microstructure, i.e. 3.09 GPa (at a 10% strain level), is higher than those of single crystals. Among the single crystalline samples, the <010> orientation under compression exhibits the highest hardening modulus of theoretically 2.58 GPa and experimentally 2.60 GPa. Following it, the hardening slopes of the <111> and <122> tension samples lay within the range of 1.8–2.0 GPa and 0.9–1.0 GPa respectively.

## 5. Discussion and implications of the results

### 5.1. Low intrinsic stacking fault energy of FeNiCoCrMn

The relative dominance of the mixing entropy over the mixing enthalpy on molar basis plays a decisive role in the disordered solid solution state of FeNiCoCrMn [56]. Therefore, any physical contribution to these two thermodynamic properties affect the solid-solubility of these five constituent elements. Even though formation of long-range ordered phases are restrained by the promoted mixing entropy, the short-range order effects on the deformation behavior of FeNiCoCrMn should be given special credit [57]. This is illustrated by the fact that the low stacking fault energy of the metastable fcc structure of Co atoms, governed by the composition function $C(x)$ in Fig. 2, stands out as a driving force for promoting slip on regions of high Co concentration. To that end, the short-range ordered regions with locally high Co concentration act as energy-wise favorable sites for the formation of faults similar to the Suzuki segregation mechanism in which case the solute atom attracted to the fault decreases the fault energy [28].

Albeit the high concentration of Co decreases the misfit energy, it also introduces a dislocation-solute interaction energy term, $E_{D-S}$, which acts as an energy penalty during the glide of twinning partials. To that end, meanwhile $E_{D-S}$term tends to promote $\tau^{M}_{crit}$, the decrease in the $\gamma$-curve levels dominate as the $E_{total}$ term is minimized for higher Co concentration in FeNiCoCrMn HEA [58]. At this stage it should be emphasized that the resultant effect of the solid solution-dislocation interaction energy and the misfit energy terms can only be resolved with the accurate quantification of the interatomic forces involved [59,60].

### 5.2. Effect of residual dislocations on twin migration stress

Meanwhile the critical stress for twin nucleation, $\tau^{N}_{crit}$, follows Schmid behavior in tension and compression; the twin migration stress, $\tau^{M}_{crit}$, shows significant deviations as detailed in Appendix C. The interaction between the incident twinning partials and the latent twin boundary holds an undisputable importance for this anisotropic behavior observed in the $\tau^{M}_{crit}$ levels. On theoretical grounds, the modification of GPFE curve upon the localization of the misfit energy-due to the $b_r$ vector-increases the critical stress level required for the migration of the latent twinning partials [24]. A similar increase in the misfit energy has been also observed for the slip-twin interaction reactions as noted by Sehitoglu et al. [39]. The slip transmission across the twin boundaries modifies $\gamma_{us}$ and stimulates a similar effect of elevation in the CRSS levels for glide along the latent slip systems [15,27]. This analogy between slip-twin and twin-twin interactions address that both the defect and the boundary structures should be elaborated in atomistic scale to build a comprehensive understanding of the twin migration kinetics in FeNiCoCrMn HEA. On the other hand, considering the smaller $b_r$ values involved, the hardening effect is expected to be smaller in magnitude for the twin-slip interaction compared to the twin-twin interaction [39].

The proposed multiscale energetics model for twin migration in Eq. (1) incorporates the interaction geometry and the dislocation reaction information via the slip vectors of primary/latent twinning partials and the *ab-initio* generated GPFE curves. To that end, this novel approach allows us to interrogate on the latent hardening within a physical framework involving interatomic forces. On numerical basis, the misfit energy is composed of $\gamma_{\text{incidentGPFE}}$ and $\gamma_{\text{modifiedGPFE}}$ profiles which are more dominant compared to the long-range dislocation line and interaction energy terms. This dominant contribution of lattice misfit energy lay bare the paramount importance of short range atomistic interactions in explaining the experimental latent hardening phenomenon in FeNiCoCrMn avoiding any empirical constants.

From the quantitative analysis presented in *Methods* section, the residual lattice disregistry, as reflected by $b_r$ and $\gamma_{\text{modifiedGPFE}}$ terms, plays a key role in $\tau^{M}_{crit}$ magnitude. The significant role of non-glide deviatoric stress components, i.e. $S_{11}$, $S_{22}$, $S_{13}$, $S_{21}$, in the non-Schmid behavior of $\tau^{M}_{crit}$ are expressed by the finite values of $a_1$, $a_2$, $a_3$ and $a_4$ yield criterion coefficients in Table C1 in Appendix C. This interplay highlights the role of the independent non-glide deviatoric stress components in addition to the unidirectional nature of twinning phenomenon in deriving a macroscale generalized

yield criterion formulation as shown in Appendix C.

The terms of the hardening matrix $[H_{\alpha\beta}]$, also cannot be solely interpreted excluding the effects of $b_r$ and $\gamma_{\text{modifiedGPFE}}$. As demonstrated by comparing Tables B1 and B2, the $H_{\alpha\beta}$ terms governed by $b_r$ and $\gamma_{\text{modifiedGPFE}}$ which interact in an intricate fashion entailing the anisotropic character of the hardening observed in the experiments. On physical grounds, the stress increments of $d\tau^M_{crit}$ and $d\tau^T_{crit}$ are governed by the variation of the corresponding $E_{total}$ expressions of Eq. (1) in response to the incremental disregistry shears, i.e. $d\gamma^{(1)}$ and $d\gamma^{(2)}$. It is to be noted that these two shear terms are closely related with the twin-twin interactions manifested by dislocation reactions in Appendix B. This attitude of $H_{\alpha\beta}$ exhibits an analogy with the slip-induced latent hardening behavior which is also experimentally observed to promote with the strength of dislocation junctions [23].

### 5.3. Comparison with experiments

Recent experimental work conducted in a number of single crystal orientations of FeNiCoCrMn have precisely established the critical twin nucleation stress, $\tau^N_{crit}$ , which is equal to 168 MPa [4]. On the other hand, significant anisotropy is observed to be present for the latent twin migration stress, $\tau^M_{crit}$. This leads to $\tau^M_{crit}/\tau^N_{crit}$ ratio vary between 1.22 in <111> orientation to 1.3 for the case of <122> orientation. The theoretical predictions are 1.25 and 1.35 for these two orientations which imply an excellent agreement with the experimental measurements.

Similar trend of anisotropy is also observed for the strain hardening slope $h_{eff}$ in uniaxial experiments. The set of tensile experiments on <111> oriented single crystals by Kireeva et al. [44] and our group (unpublished work and [4]) show a high strain hardening slope of 1.8−1.9 GPa in FeNiCoCrMn HEA which is in perfect agreement with our theoretical predictions of 1.82 GPa. Furthermore, the <010> compression experiments exhibit $h_{eff}$ value of 2.58 GPa complies closely with the theoretical level of 2.71 GPa. For the polycrystalline sample, $h_{eff}$ is evaluated to be more pronounced compared to the single crystalline cases. This theoretical result is further confirmed to lay within the experimental measurement range recently conducted by our group and to be published. In this case, the compatibility requirements imposed by the grains are expected to promote residual slip and elevate $h_{eff}$ slope.

The close correspondence between the theoretical predictions and the experimental measurements indicates that our current modelling approach is capable of capturing the physical mechanisms accompanying the twin nucleation and migration phenomena. The earlier phenomenological approaches which are based on empirical parameterization of the self and latent hardening coefficients are of limited versatility and do not reflect the intrinsic properties of twinning such as non-Schmid effects or the anisotropy involved in the twinning dislocation reactions and the elastic constants involved. In order to build a comprehensive understanding on these physical aspects of the twin migration and the associated hardening phenomena, in this work, we put special emphasis on the adaptive character of the mechanical formulations. To that end, the incorporation of the atomistic scale fault energetics into the mesoscale twinning dislocation interactions involving the migration reactions and the short-range solute concentration effects plays a key role in the close agreement between the theoretical predictions and experimental measurements. Furthermore, the model is extended to be applicable to both single- and poly-crystalline samples employing the crystal plasticity theory.

The formulation we presented can be further extended to analyze the twin-slip as well as slip-slip interactions. However, the experimental data collected on FeNiCoCrMn HEA at 77 K for pure slip and slip-twin cases exhibit much lower hardening slope. Hence the latent hardening is expected to be less pronounced in these two interaction mechanisms compared to the crossing twin configurations [4]. This experimental observation complies with the smaller $b_r$ vectors associated with the slip-slip [47,48,61] and twin-slip interactions [23,62] compared to the twin-twin interactions [23,62] addressing the significance of the undergoing dislocation reactions.

### 5.4. Potential application of the proposed model in crystal plasticity

Recent crystal plasticity methods adopted on modelling the twin nucleation and migration in close packed crystallite necessitates an accurate quantification of the corresponding stress levels to be incorporated in the constitutive framework. Identification of $\tau^N_{crit}$, $\tau^T_{crit}$ and $\tau^M_{crit}$ stresses via the multiscale energy scale formulation developed in this work aims to fulfill this need. Furthermore, the self and latent hardening moduli calculated based on mutual interaction of primary and latent twins serve as reflections of the on-going meso-scale dislocation reactions into the macroscopic stress-strain behavior. As previously noted in the earlier literature on experimental grounds [62−64], the mutual twin interactions described based on twinning partial dislocation reactions are decisive in the resulting migration stress levels. Entailing a realistic material response in the full-field crystal plasticity approaches necessitates a systematic data set depicting the twin interaction geometry and the flow stress levels. To that end, the derived flow stress levels along with the hardening moduli serve as indispensable constitutive inputs for FeNiCoCrMn HEA which is distinguishing with its prominent twinning tendency linked with its low stacking fault energy. Moreover, the accurate determination of flow stress levels has important extensions to the realistic prediction of the evolving twinning morphology in a microstructure, such as the energetic favorability of a thickening single twin or the nucleation of multiple twin lamella [51].

In light of the results given in this paper, the twin nucleation stress, $\tau^N_{crit}$ , is governed by the resolved shear stress, acting along the twinning system considering the unidirectional nature of the twinning crystallography. On the other hand, the migration of the primary and latent systems, initiating at the resolved shear stress levels of $\tau^T_{crit}$ and $\tau^M_{crit}$, exhibit anisotropic character owing to the presence of $b_r$ and the mutual twin interaction geometry. Therefore, similar anisotropy is also reflected in both self and latent hardening components of the hardening matrix $[H_{\alpha\beta}]$ as demonstrated in Table 4 and Table B2 complying with the experimental measurements.

For the purposes of crystal plasticity implementation, it is recommended to use the twin migration stress equation, i.e. Eq. (C3) in Appendix C, as a first approximation to quantify the macroscopic flow stress and the hardening matrix, $[H_{\alpha\beta}]$, for the hardening response. The twin migration stress formulation already accounts for the orientation dependence of flow stress which can be substantial in view of the twin intersections at the incipient stages of flow. For example, near the <010> pole in compression, the twin intersection could initiate readily in view of multiple twin systems of having same *SF*'s. Similarly, near the <111> pole in tension, multiple systems can be activated rendering the use of the migration equation Eq. (C.3) of Appendix C at the earlier stages of the flow. Similar conclusions can be also drawn for the polycrystalline case. Note that as deformation proceeds the number of active systems will likely increase which is naturally incorporated in the model capabilities.

The methodology employed for the derivation of the latent hardening coefficients differs naturally from the earlier literature which focuses on slip-induced hardening effects [25,27]. By consideration of the mutual interaction of two systems, the

analytical approach undertaken is able to isolate the twin-twin interactions and avoids the complexities associated with extraction of the empirical parameters from the experimental measurements in which case more than two systems may interact and affect the dominant behavior. Once the mutual 2-combination twin interactions are established, the formulation can be generalized to predict the hardening slope $h_{eff}$ for higher number of twins as demonstrated in Table 4. At this stage, it is to be emphasized that similar theoretical concepts can be also adopted to the twin migration induced hardening in body centered cubic [29,30,65] and hexagonal close packed metals [66,67] as they are also known to exhibit significant non-Schmid behavior and hardening during twinning similar to fcc structured FeNiCoCrMn HEA focused in this study.

We note that our treatment of the latent hardening did not require the specification of the volume fraction of twinning (except the polycrystalline case). This is in view of the fact that the hardening matrix coefficients are derived from the mutual interactions of two twins, and the accompanying incremental changes in stress and strain increments. Once the hardening coefficients are established, they can be utilized in conjunction with different flow rules for twinning. Naturally, the overall plastic strain rate that should be utilized in a crystal plasticity formulation must ensure that the plastic strain rate is the product of volume fraction times the intrinsic twinning shear [51,52]. As we incorporated the twinning partial reactions for migration and quantify the modifications introduced on the corresponding energy terms, the volume fraction magnitude in the determination of the hardening coefficients is not invoked for double twin interactions. The adopted volume-fraction invariant analysis finds its roots in the mutual interaction induced latent hardening being dependent on $b_r$ and the $E_{total}$ variation.

The approach presented in the current work extended the previous treatments in the following ways: (1) previous works have used the same form of the hardening matrix irrespective of whether the strain hardening stems from twin-slip, twin-twin and slip-slip interactions and treated the latent hardening coefficients to be identical without distinguishing the dislocation reactions ongoing in these distinct hardening mechanisms. As experimentally tracking the individual hardening coefficients is a very strenuous task, it was reasonable to infer a single fitting parameter. On the other hand, the current work follows a novel methodology illustrating that the resulting Burgers vectors exhibit significant differences in response to the specific twin systems that interact. To that end, the latent hardening coefficients display a strong anisotropy on a case by case basis as illustrated in Table B2. (2) the current paper clearly shows how the twin self-hardening in the primary and latent systems differ as well demonstrated in Fig. 1 and provides the governing equations for describing the magnitudes of the diagonal twin self-hardening terms which are unequal unlike the assumption in previous studies, and finally (3) the present consideration views the contributions from slip-slip and slip-twin to be small relative to twin-twin hardening cases. In the case of twin-slip interaction, the corresponding hardening can be discussed on two main pillars: (i) previous works assess the increase in slip induced hardening linked with the increase in twin density (arising from reduction in the mean free path for slip) but this effect is again considered to be small compared to twin-twin induced strengthening, and (ii) the methodology in the present work can be also adopted to the slip-twin interactions employing the calculated residual Burgers vectors associated with the dislocation reactions in the earlier works by our group [39,40] and one could obtain the twin hardening resulting from this type of an interaction (not discussed in previous works), but again the contribution falls far short of the twin-twin induced hardening.

In summary, the current study represents an elucidation of the overwhelming role of twin-twin interactions on strain hardening in the fcc FeMnNiCoCr alloys. In general, the strengthening originates from five causes- (i) self hardening due to isolated slip, (ii) self hardening due to twinning, (iii) latent hardening due to slip-slip interaction, (iv) latent hardening via slip-twin interaction and (v) latent hardening under twin-twin interactions. In the case of high stacking fault energy alloys such as Ni, only (i) and (iii) are operative, as stresses levels for twinning could not be reached. For the case of very low stacking fault fcc alloys, such as FeMnNiCoCr in this study, the twinning mechanism can prevail. Hence, depending on the crystal orientation all of the (i)-(v) mechanisms can be active. However, when (v) is present, it dominates the magnitude of strain hardening almost in its entirety. Due to contribution from (v) alone, ie. twin-twin interactions, we accounted for the correct strain hardening moduli that compares favorably to experiments. Our calculations for the twin-slip case (iv) lead to smaller Burgers vectors and strain hardening magnitudes less than 0.07 times of case (v) in this study.

## 6. Conclusions

We draw the following conclusions from the current work:

(i) We derived the twin migration stress for the primary and latent twins and constructed the latent hardening matrix for the twin-twin interactions in FeNiCoCrMn high entropy alloy based on the atomic scale calculations and the meso-scale twinning partial reactions. Incorporating the energetics obtained from *ab-initio* DFT calculations with the elastic interactions of the twinning dislocations resulted in strain hardening coefficients in excellent agreement with experiments.

(ii) Short range ordering associated with the increase of the Co concentration is demonstrated to facilitate the twining via lowering the GPFE energy barriers.

(iii) The established latent hardening matrix predicts the correct trends observed in the experiments for uniaxial <010> compression and <111>, <123> and <122> tension as well as the polycrystalline cases. Both self and latent hardening terms contribute to the overall prediction of the hardening slope.

(iv) A generalized twin migration stress criterion was developed for the high entropy alloy of FeNiCoCrMn. The yield criterion is capable of encompassing both the glide and non-glide stress components in close agreement with the experiments.

## Acknowledgements

The work is supported by NSF-CMMI 15-62288 which is gratefully acknowledged.

## Appendix A. Derivation of twin nucleation stress $\tau^N_{crit}$

This appendix section focuses on the calculation of the critical stress for the twin nucleation, $\tau^N_{crit}$. In this work, the twin nucleation analysis is established based on the three-layered dislocation arrangement of a twin nucleus in Fig. A1 following the results of the earlier works in references of [29,38,68]. In this configuration, the twinning partial dislocation $A$ is positioned at $r_A$, where as the dislocations $B$ and C are positioned at $r_B$and $r_C$. Thus, the separation distances $d_1$ and $d_2$ correspond to $d_1 = r_A - r_B$ and $d_2 = r_C - r_B$. The total energy of the twin configuration in Fig. A1 can be written as the summation of the individual line energies of the twinning partials, the interaction energies of the partials among themselves and the solute atoms as well as the misfit energy due to the atomic

scale neighborhood change and the applied work done on the twinning partials:

$$E_{total} = E_{self} + E_{\text{inter}} + E_{misfit} + E_{D-S} - W = N\frac{Kb_1^2}{2\pi}\ln\left(\frac{r_A - r_B}{\xi}\right) - \frac{Kb_1^2}{2\pi}\left(\ln\frac{r_A - r_B}{\xi} + \ln\frac{r_B - r_C}{\xi} + \ln\frac{r_A - r_C}{\xi}\right) + \sum_{m=-\infty}^{\infty}\gamma_{incidentGPFE}a' + \int C(x)\sigma_{ij}^{disl}\varepsilon_{ij}^{*}dV - \tau_{crit}^{N}b_1A_1 \quad (A.1)$$

Here N represents the number of twinning partials forming the twin nucleus, i.e. equal to 3, and $K$ is an anisotropic constant which has been evaluated by Foreman [69] for a screw dislocation in an anisotropic cubic crystal as follows:

$$K = \sqrt{\frac{C_{44}(C_{11} - C_{22})}{2}} \quad (A.2)$$

where the elastic constants of FeNiCoCrMn are evaluated to be equal to: $C_{11} = 221$ GPa, $C_{12} = 152$ GPa, $C_{44} = 165$ GPa following the lattice energy variation in response to the different distortion (strain) components [70].

The misfit energy, $E_{misfit}$, is determined by employing the GPFE curve generated in Fig. 2. At this stage, it should be noted that $E_{misfit}$ term is a function of the spatial disregistry distribution, i.e. $\gamma_{incidentGPFE} : \gamma_{incidentGPFE}\,(f\,(ma' - u))$. The disregistry function $f(ma' - u)$represents the inelastic slip distribution introduced within the presence of the twinning partial and gives a measure of the relative displacement of the upper half of the crystal with respect to the lower half across the twin plane. The function $f : f\,(ma' - u)$ is expressed in terms of the dislocation position $u$, and the inter-planar distance $a'$ normal to the glide direction on the twin plane. It should be noted that this formulation of disregistry is capable of encompassing the discrete lattice structure via the integer multiplier factor m [71]. The solution to the disregistry function has been proposed for a twin nucleus in an fcc crystal as follows [37]:

$$f(ma' - u) = \frac{b}{\pi}\left(\tan^{-1}\left(\frac{ma' - u}{\xi}\right) + \tan^{-1}\left(\frac{ma' - u - d_1}{\xi}\right) + \tan^{-1}\left(\frac{ma' - u - (d_1 + d_2)}{\xi}\right)\right) \quad (A.3)$$

Following the description of the function of $f\,(ma' - u)$, the term of $\gamma_{incidentGPFE}$ is expanded in a piecewise-smooth sinusoidal series form of:

$$\gamma_{incidentGPFE} = \begin{cases} 0 \le \lambda \le 1.5 & \gamma_{us}\sin(0.5\pi\lambda) \\ 1.5 \le \lambda \le 2 & \frac{\gamma_{us} + \gamma_{isf}}{2} + \frac{\gamma_{us} - \gamma_{isf}}{2}\sin(2\pi\lambda - 1.25) \\ 2 \le \lambda \le 2.5 & \frac{\gamma_{ut} + \gamma_{isf}}{2} + \frac{\gamma_{ut} - \gamma_{isf}}{2}\sin(2\pi\lambda - 1.25) \\ 2.5 \le \lambda & \frac{\gamma_{ut} + 2\gamma_{tsf}}{2} + \frac{\gamma_{ut} - 2\gamma_{tsf}}{2}\sin(2\pi\lambda - 1.25) \end{cases} \quad (A.4)$$

where $\lambda = u_x/b$.We minimize the total energy expression of (A.1) with respect to the positions of the dislocations $r_A$ and $r_B$ on the verge of twinning as expressed in Eq. (A.5) and (A.6) [38]:

$$\frac{\partial E_{total}}{\partial r_A} = 0 \quad (A.5)$$

$$\frac{\partial E_{total}}{\partial r_B} = 0 \quad (A.6)$$

Simultaneous solution of Eq. (A.5) and (A.6) leads to the following expressions:

$$\frac{Kb^2}{2\pi}\left(\frac{1}{r_A - r_B} - \frac{1}{r_A}\right) - \tau_{crit}^{N} + \gamma'_{twin} = 0 \quad (A.7)$$

$$\frac{Kb^2}{2\pi}\left(\frac{1}{r_B} + \frac{1}{r_A}\right) - \tau_{crit}^{N} + \gamma'_{twin} = 0 \quad (A.8)$$

where $\gamma'_{twin}$ is defined as:

$$\gamma'_{twin} = \left(\frac{\gamma_{ut} + \gamma_{isf}}{2}\right)\sin(2.6\pi) + \left(\frac{\gamma_{ut} - \gamma_{tsf}}{2}\right)\sin(2\pi(N - 1.2)) \quad (A.9)$$

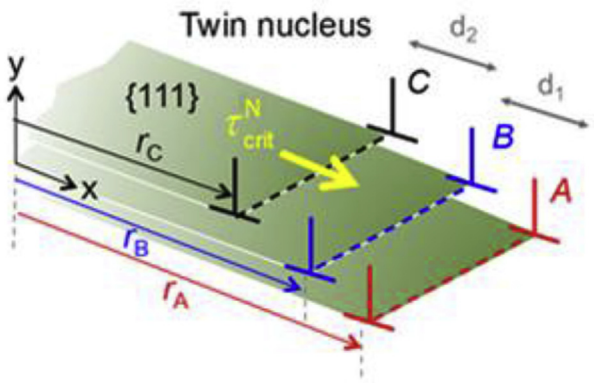


**Fig. A1.** Dislocation configuration of a three-layered twin nucleus in an fcc alloy.

At this stage, it is important to note that the resulting expressions in Eqs. (A.7) and (A.8) do not incorporate the dislocation core half-width $\xi$, and hence our calculations are independent of the value of $\xi$. For the twin nucleus shown in Fig. A1, the position $r_B$ is calculated from the simultaneous solution of Eq. (A.7)-(A.8) as follows:

$$r_B = \frac{3Kb^2}{2\pi\gamma'_{twin}} \tag{A.10}$$

It is to be noted that under zero external stress $r_B = 2r_A$. Within the presence of external stress, the leading partial A, shown in Fig. A1, is most likely to initiate glide motion. At the instant the twinning partials start gliding, the ratio of the separation distances $r_A/r_B$ is evaluated to be:

$$\frac{r_A}{r_B} = \sqrt{3} - 1 = 0.732 \tag{A.11}$$

Eq. (A.11) suggests that a twin nucleates when the ratio of $r_A/r_B$ increases to 0.732 from the external stress-free configuration of $r_A/r_B = 0.5$ [29]. Regarding the numerical values, the twinning energetics involved in Eq. (A.1), the twinning partial positions are evaluated to be as $r_B = 46\,\mathring{A}$ and $r_A = 66\,\mathring{A}$. Therefore, the separation distances $d_1$ and $d_2$ are equal to 20 $\mathring{A}$ and 46 $\mathring{A}$ respectively. It is important to point out that the separation distances $d_1$ and $d_2$ are not equal, but rather $d_1$ is smaller than $d_2$. The resulting separation distances suggest that the twin front is of a semi-lenticular shape in FeNiCoCrMn HEA complying with the experimental measurements in several other alloys [72,73].

Overall, from our calculations, we observe that separation distances largely influence $\tau^N_{crit}$ and hence accurate prediction of $d_1$ and $d_2$ are of paramount importance. Referring back to Eq. (A.1), several findings are noted. As the separation distance $d_1$ and $d_2$ deviate from the stress-free values, the interaction energy changes rapidly. On specific grounds, as $d_1$ and $d_2$ increase with the applied work, the interaction energy for the twinning partials decreases preserving the convexity of $E_{total}$ term which is exploited in Eq. (A.1) to evaluate the modified equilibrium configuration.

The *ab-initio* generated GPFE curve is modified within the presence of $b_r$ at the twin-twin interaction site. As a result, the $E_{misfit}$ term increases in value complying with the localized stress-field associated with $b_r$ . The role of $b_r$ on twin migration has been investigated in section 3 in detail. In this appendix section, we will provide supplementary quantitative arguments on the elevation of the energy barrier from $\gamma_{ut}$ to $\gamma^{\text{mod}}_{ut}$ which in turn leads to the amplification of $\tau^M_{crit}/\tau^N_{crit}$ ratio with $b_r$ as shown in Fig. 4. The $\gamma_{\text{modifiedGPFE}} : \gamma_{\text{modifiedGPFE}}(\lambda)$ can expressed in analytical form within the range of $3 \le \lambda \le 4$for the particular case of $b_r = 0.82$:

$$\gamma_{\text{mod}ifiedGPFE}(\lambda) = \frac{\gamma^{\text{mod}}_{ut} + \gamma_{tsf}}{2} + \left(\frac{\gamma^{\text{mod}}_{ut} + \gamma_{tsf}}{2}\right)\sin[2\pi\lambda - 1.2] \tag{A.12}$$

Fig. A2 provides a comparison of the modified GPFE for the particular cases of $b_r = 0$ and$b_r = 0.82$ a. As can be seen significant increase in the energy barrier levels are introduced as a result of promotion in the disregistry vector $b_r$. This modification in the GPFE curve is also reflected in the $\tau^M_{crit}$ value and plays a pivotal role in the resulting hardening behavior of FeNiCoCrMn HEA.

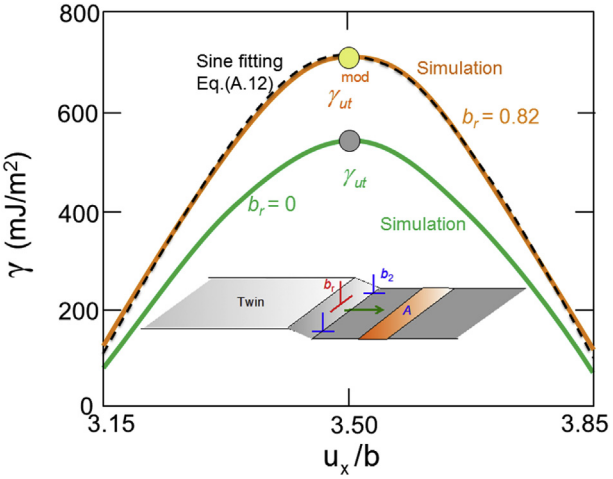


**Fig. A2.** Effect of the residual dislocation on $\gamma_{ut}$ value in FeNiCoCrMn. The modified GPFE curve based on Eq. (A.4) and (A.12) are also shown by broken black lines.

## Appendix B. Derivation of hardening coefficients at the microstructural level

In this section, we put emphasis on the construction of hardening matrix, i.e. $[H_{\alpha\beta}]$, the components of which are determined based on the two-by-two mutual twin interaction combinations. In order to accomplish this task; firstly, we focused on the possible geometry of the twin-twin interactions. Traditionally, Thompson tetrahedron, shown in Fig. B1, has proved itself very instrumental in visualization of the possible reactions incurring among the twinning partials in fcc structures such as the case of FeNiCoCrMn HEA. The faces of the Thompson tetrahedron (ABC, BCD, ACD and ABD) represent the close-packed slip and twin planes in the fcc lattice while the edges of the tetrahedron (for example AB, AC, AD, BC etc.) extending from one vertex to another represent the close-packed slip directions belonging to the {111} <110> systems. The centers of the Thompson tetrahedron are represented by Greek symbols $(\alpha, \beta, \delta, \gamma)$corresponding the label of the opposite vertex, which represent the {111}<112> partial dislocations. For example, the vectors $B\delta$ and $\beta D$ represent the$(111)\left(\bar{2}11\right)$and $\left(\bar{1}11\right)(211)$systems respectively. The tetrahedron illustrates the four possible twin planes $(11\bar{1})$ (111), $(\bar{1}11)$ and $(1\bar{1}1)$ with the three possible <112> twinning directions on each plane, constituting a total of 12 possible twin systems (see Table 1). At this stage, the unidirectional nature of the twinning should be also given special credit.

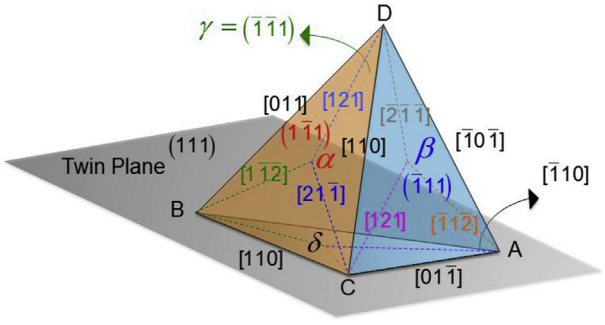


**Fig. B1.** Thompson tetrahedron showing possible twin systems in an fcc crystal. The broken colored lines drawn following the color convention used in Table 1 show <112> twinning directions.

It is to be noted that a {111} <112> partial dislocation may cross-slip onto the conjugate {111} twin planes as a result of dislocation-twin boundary interactions involving incorporation, transmission

and blockage [23,49]. In this work, we focus on the particular set of reactions which introduce latent twin migration. On mechanical grounds, the partial dislocations on the primary twin system interact with the latent twin boundary entailing the activation of the latent twin system by the glide of latent system partials. Consequently, this interaction leaves $b_r$ vector at the interaction site obeying the conservation Burgers vector.

Fig. B2, shows a Scanning Electron Microscope (SEM) image for a single crystal of equiatomic FeNiCoCrMn with the shown $[\bar{1}1\bar{1}]$ orientation loaded in tension. The sample is homogenized at 1473 K for 24 h and solutionized at 1373 K for 1hr. Both the orientations of the pristine and deformed samples are confirmed by Electron Back Scatter Diffraction (EBSD). The details of the experimental work will be provided in a prospective work and therefore it is beyond the scope of this paper. On the other hand, the SEM image provides experimental evidence for the interaction of the primary $(\bar{1}11)$ $[\bar{1}1\bar{2}]$ twin system ($SF_1$=0.32) with the latent system of $(11\bar{1})$ $[\bar{1}\,\bar{1}\,\bar{2}]$ ($SF_2$ = 0.16) at the area of interest which is framed in red color and is particularly important to supplement the theoretical analysis presented in this work. The twin migration on the primary system blocked by the latent twin boundary acts as a migration site for the latent twin system and contributes to the overall hardening under proceeding deformation. The $b_r$ value is evaluated to be of 0.82 a (the derivation will be detailed in following analysis in Table B1) which significantly contributes to the latent hardening level of 0.34 GPa per unit shear stress increment attributed to the sample. To that end, as supplemented by this experimental evidence, the latent hardening effects in FeNiCoCrMn HEA should be incorporated into any modelling efforts on twinning induced plasticity.

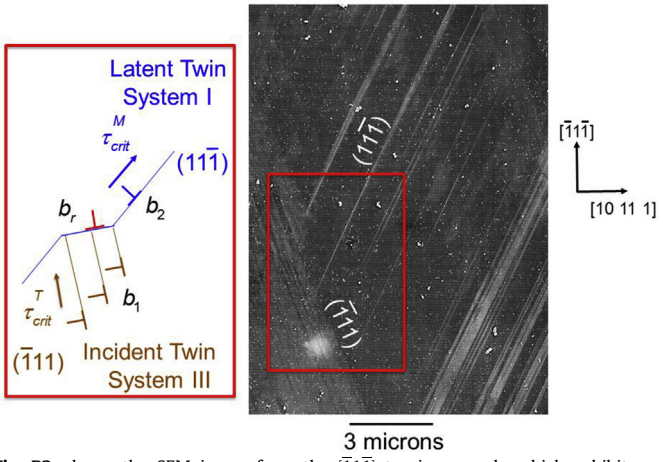


**Fig. B2.** shows the SEM image from the $[\bar{1}1\bar{1}]$ tension sample which exhibits an example of the interaction between the primary and the latent twin systems of $(\bar{1}11)$ $[\bar{1}1\bar{2}]$and $(11\bar{1})$ $[\bar{1}\,\bar{1}\,\bar{2}]$, respectively. On theoretical grounds, this twin-twin interaction is calculated to contribute a resolved shear stress level of 0.34 GPa to $\tau^M_{crit}$ in unit shear strain increment which plays a prominent role on the plastic deformation of FeNiCoCrMn HEA.

To exemplify the procedure followed in evaluating the hardening coefficients $H_{\alpha\beta}$, we will present a demonstration in which case we consider only two twin systems, i.e. primary twin: $(111)\left(1\bar{2}1\right)$and the latent twin $(\bar{1}11)[211]$ systems. For this particular case, the primary twin nucleus is composed of $3\,\mathrm{x}\,a/6\left(1\bar{2}1\right)$ partials. These three twinning partials in the primary system interact with the latent system following the set of reactions shown in Eq. (B.1) and (B.2) [62,68]:

$$\underbrace{3\,\mathrm{x}\,\frac{a}{6}\left(1\bar{2}1\right)}_{\text{Primary Twin}} \rightarrow \underbrace{\frac{a}{2}(110)+\frac{a}{2}(101)}_{\text{Latent Twin}} + \underbrace{2\,\mathrm{x}\,\frac{a}{6}(121)}_{\text{Residual}} \tag{B.1}$$

$$\underbrace{\frac{a}{2}(110)+\frac{a}{2}(101)}_{\text{Latent Twin}} \rightarrow \underbrace{3\,\mathrm{x}\,\frac{a}{6}(211)}_{\text{Latent Twin}} \tag{B.2}$$

The plastic shear strains $\gamma^{(1)}$ and $\gamma^{(2)}$ are the strains associated with the motion of twinning dislocations on the primary and latent twin systems, and can be evaluated from the geometrical definition of the twinning shear [74]. Among these two strain levels, $\gamma^{(1)}$ on the primary twin system can be evaluated employing the relation:

$$\gamma^{(1)} = b\Big/d_{\{111\}} - \tau^T_{crit}\Big/\mu_{\{111\}<112>} \tag{B.3}$$

where $\tau^T_{crit}$ is the CRSS for the primary twin migration and $b_1$ is equal to $|3\,\mathrm{x}\;a/6<112>|$. As the elastic strain is much lower than the plastic strain, $\gamma^{(1)}$ term can be approximated as $b/d_{\{111\}}$which is the twinning strain. On the other hand, the plastic shear strain $\gamma^{(2)}$ on the latent twin system is modified by the residual slip vector $b_r$ and can be expressed as in Eq. (B.4) (neglecting the elastic strain term):

$$\gamma^{(2)} = (b+b_r)/d_{\{111\}} \tag{B.4}$$

The term $\gamma^{(1)}$ on the primary twin system is 0.70 and the term $\gamma^{(2)}$ on the latent twin system is 2.12 using a value of $b_r$ = 0.82 a. As there are two systems active, the resulting hardening matrix will be of $2\times2$ dimensions which is a minor of the general $12\times12$ hardening matrix$[H_{\alpha\beta}]$. Adapting the strain rate-independent crystal plasticity formulation of Eq. (8) for this particular case, the increments of twin migration stresses are related to the shear strain increments as follows:

$$d\tau^T_{crit} = H_{11}d\gamma^{(1)} + h_{12}d\gamma^{(2)} \tag{B.5}$$

$$d\tau^M_{crit} = h_{21}d\gamma^{(1)} + H_{22}d\gamma^{(2)} \tag{B.6}$$

Expressing the off-diagonal terms $h_{12} = qH_{11}$ and $h_{21} = qH_{22}$ where $q$ is a constant ranging from 0 to 1 following the analogous relationship between the self-hardening moduli $H_{22}$and $H_{11}$ that has been proposed for the slip-induced latent hardening follows as [25,75,76]:

$$(H_{22}/H_{11}) = \Gamma(\mathrm{M}-q)/(1-q\mathrm{M}) \tag{B.7}$$

In Eq. (B.7), $\Gamma$ is the ratio of the shear strains between the primary and the latent twin, i.e. $\Gamma = d\gamma^{(1)}/d\gamma^{(2)}$, and $M$ is the ratio of the $SF$'s corresponding to the latent and primary twin systems. For $q \ll \mathrm{M} \ll 1$, which is generally the case for the annealed crystalline [25], Eq. (B.7) turns out to be equivalent to:

$$H_{22}/H_{11} = \Gamma M \tag{B.8}$$

The construction of hardening matrix necessitates determination of the parameter $q$ and the hardening coefficient $H_{11}$. These two unknowns are evaluated by the variation of shear disregistries of $d\gamma^{(1)}$ and $d\gamma^{(2)}$ are equal to 0.06% and 0.12%. From the simultaneous solution of Eq. (B.5) and (B.6), the values of these two unknown constants are determined as $q$ = 0.32 and $H_{11}$ = 1.4 GPa. Therefore, the $2\times2$ hardening matrix for this specific interaction geometry between the primary $(111)\left(1\bar{2}1\right)$and the latent $(\bar{1}11)[211]$ twin systems is constructed as:

$$\left[H_{\alpha\beta}\right] = \begin{bmatrix} 1.4 & 0.45 \\ 0.45 & 1.4 \end{bmatrix} \text{GPa} \tag{B.9}$$

In Table B1, we generalized this approach for the possible mutual twin-twin interactions in an fcc crystal. For designations of the twin systems, refer to Table 1. Furthermore, the variation of the $b_r$ vector based on the interacting twins is tabulated in Table B2. The diagonal components in both Tables B1 are zero as no residual dislocations are present when a single twin system is activated and the hardening results from the pile-up effect of the twinning partials. Overall, from Table B1, we infer that the residual dislocation magnitudes range from 0.54a to 1.22a contributing to the high strain hardening in fcc FeNiCoCrMn HEA. It should be emphasized that the anisotropy involved in the $b_r$ vector magnitudes is similarly reflected in the hardening slopes as tabulated in Table 4 and Table B2.

**Table B1**
The normalized residual dislocation $(b_r/a)$ due to possible twin-twin interactions in FeNiCoCrMn alloy.

| | I | II | III | IV | V | VI | VII | VIII | IX | X | XI | XII |
|---|---|---|---|---|---|---|---|---|---|---|---|---|
| I | 0 | 0.70 | 0.82 | 0.82 | 1.22 | 1.22 | 0.59 | 0.59 | 0.70 | 0.70 | 0.59 | 0.82 |
| II | 0.70 | 0 | 0.59 | 1.22 | 0.82 | 0.82 | 0.54 | 1.22 | 0.70 | 0.70 | 0.59 | 1.22 |
| III | 0.82 | 0.59 | 0 | 0.70 | 0.70 | 0.59 | 0.82 | 0.82 | 0.82 | 1.22 | 1.22 | 1.22 |
| IV | 0.82 | 1.22 | 0.70 | 0 | 0.70 | 0.59 | 0.82 | 0.70 | 1.22 | 0.70 | 0.70 | 0.59 |
| V | 1.22 | 0.82 | 0.70 | 0.70 | 0 | 1.22 | 1.22 | 0.82 | 0.59 | 0.59 | 0.54 | 1.22 |
| VI | 1.22 | 0.82 | 0.59 | 0.59 | 1.22 | 0 | 0.82 | 0.82 | 0.59 | 1.22 | 1.22 | 0.59 |
| VII | 0.59 | 0.54 | 0.82 | 0.82 | 1.22 | 0.82 | 0 | 1.22 | 0.82 | 0.70 | 1.22 | 0.59 |
| VIII | 0.59 | 1.22 | 0.82 | 0.70 | 0.82 | 0.82 | 1.22 | 0 | 0.59 | 0.82 | 0.82 | 0.82 |
| IX | 0.70 | 0.70 | 0.82 | 1.22 | 0.59 | 0.59 | 0.82 | 0.59 | 0 | 1.22 | 1.22 | 0.82 |
| X | 0.70 | 0.70 | 1.22 | 0.70 | 0.59 | 1.22 | 0.70 | 0.82 | 1.22 | 0 | 0.82 | 0.70 |
| XI | 0.59 | 0.59 | 1.22 | 0.70 | 0.54 | 1.22 | 1.22 | 0.82 | 1.22 | 0.82 | 0 | 0.70 |
| XII | 0.82 | 1.22 | 1.22 | 0.59 | 1.22 | 0.59 | 0.59 | 0.82 | 0.82 | 0.70 | 0.70 | 0 |

**Table B2**
Hardening moduli $(H_{\alpha\beta})$ in GPa due to possible twin-twin interactions in FeNiCoCrMn high entropy alloy.

| | I | II | III | IV | V | VI | VII | VIII | IX | X | XI | XII |
|---|---|---|---|---|---|---|---|---|---|---|---|---|
| I | 1.4 | 0.45 | 0.34 | 0.34 | 0.92 | 0.92 | 0.54 | 0.54 | 0.45 | 0.45 | 0.54 | 0.34 |
| II | 0.45 | 1.4 | 0.54 | 0.92 | 0.34 | 0.34 | 0.54 | 0.92 | 0.45 | 0.45 | 0.54 | 0.92 |
| III | 0.34 | 0.54 | 1.4 | 0.45 | 0.45 | 0.54 | 0.34 | 0.34 | 0.34 | 0.92 | 0.92 | 0.92 |
| IV | 0.34 | 0.92 | 0.45 | 1.1 | 0.45 | 0.54 | 0.34 | 0.45 | 0.92 | 0.45 | 0.45 | 0.54 |
| V | 0.92 | 0.34 | 0.45 | 0.45 | 1.1 | 0.92 | 0.92 | 0.34 | 0.54 | 0.54 | 0.54 | 0.92 |
| VI | 0.92 | 0.34 | 0.54 | 0.54 | 0.92 | 2.4 | 0.34 | 0.34 | 0.54 | 0.92 | 0.92 | 0.54 |
| VII | 0.54 | 0.54 | 0.34 | 0.34 | 0.92 | 0.34 | 2.4 | 0.92 | 0.34 | 0.45 | 0.92 | 0.54 |
| VIII | 0.54 | 0.92 | 0.34 | 0.45 | 0.34 | 0.34 | 0.92 | 1.1 | 0.54 | 0.34 | 0.54 | 0.34 |
| IX | 0.45 | 0.45 | 0.34 | 0.92 | 0.54 | 0.54 | 0.34 | 0.54 | 1.4 | 0.92 | 0.92 | 0.34 |
| X | 0.45 | 0.45 | 0.92 | 0.45 | 0.54 | 0.92 | 0.45 | 0.34 | 0.92 | 1.8 | 0.34 | 0.45 |
| XI | 0.54 | 0.54 | 0.92 | 0.45 | 0.54 | 0.92 | 0.92 | 0.54 | 0.92 | 0.34 | 1.1 | 0.45 |
| XII | 0.34 | 0.92 | 0.92 | 0.54 | 0.92 | 0.54 | 0.54 | 0.34 | 0.34 | 0.45 | 0.45 | 1.8 |

## Appendix C. The anisotropy in twinning migration criterion

The theoretical analysis introduced in this work indicates that the latent twin migration stress, $\tau^{M}_{crit}$, is higher than the twin nucleation stress, $\tau^{N}_{crit}$ as an outcome of the mutual twin interactions. In particular, for any given two loading orientations, there is no proportional relationship between the elevation in $\tau^{M}_{crit}$ and $\tau^{N}_{crit}$stresses addressing the complicated nature of the undergoing physical mechanisms. Both the theoretical and the experimental values clearly reflect the deviation of $\tau^{M}_{crit}$ stress from the Schmid law as a function of crystal orientation and loading sense. Based on these arguments, in this appendix section, our main goal is to construct a generalized yield criterion which can encompass the anisotropy observed in $\tau^{M}_{crit}$.

The yield criterion for twin migration is constructed based on the atomistically-informed calculations addressing that not only the glide shear stress component but the complete stress tensor, $[\sigma_{ij}]$ (i,j = 1,2,3), acting on the twin systems dictates $\tau^{M}_{crit}$. The deviatoric stress components, $S_{ij} = \sigma_{ij} - (1/3)\,\text{trace}(\sigma_{kk})$ (i,j,k = 1,2,3), are constructed with the knowledge of the loading direction and the activated twin system. This is illustrated in Fig. C1 where the sample coordinate frame is represented by $X_1 - X_2 - X_3$ along with the orthonormal basis vectors of $e_1$, $e_2$ and $e_3$ in this frame. Similarly, the coordinate frame of the active twin system is described by $x_1 - x_2 - x_3$ with the orthonormal basis of $e'_1$-$e'_2$-$e'_3$. Among these three base vectors, while $e'_2$ is parallel to the twin plane normal and $e'_3$ is selected as parallel to the twinning direction. For a given uniaxial loading direction parallel to $X_2$axis, the stress state on the twin plane can be obtained by the transformation matrix, [**Q**] as follows:

$$(\mathrm{Q}) = \begin{pmatrix} e'_1\cdot e_1 & e'_1\cdot e_2 & e'_1\cdot e_3 \\ e'_2\cdot e_1 & e'_2\cdot e_2 & e'_2\cdot e_3 \\ e'_3\cdot e_1 & e'_3\cdot e_2 & e'_3\cdot e_3 \end{pmatrix} \tag{C.1}$$

Then following the second order tensor transformation rules, the transformed deviatoric stress tensor can be deduced for each loading orientation as follows:

$$S'_{ij} = Q_{ik} S_{km} Q^{T}_{mj} \tag{C.2}$$

where $S'_{ij}$ is the ij$^{th}$ component of the deviatoric stress in the twin coordinate frame. In the current work, we first obtained the deviatoric stress components for each orientation outlined in Table 4.

$$\tau^{*}_{cr} = \underbrace{S_{23}}_{\tau^{M}_{crit}} + a_1 S_{11} + a_2 S_{22} + a_3 S_{12} + a_4 S_{13} \tag{C.3}$$

The coefficients $\{a_1, a_2, a_3, a_4\}$ in Eq. (C.3) are evaluated by multi-linear regression and provided in Table C1. The terms other than the glide shear stress $S_{23}$ in Eq. (C.3) - $S_{11}$ , $S_{22}$, $S_{21}$ and $S_{13}$ are referred to as “non-glide stresses”. To that end, the generalized yield criterion is composed of both “glide” and “non-glide” stress components.

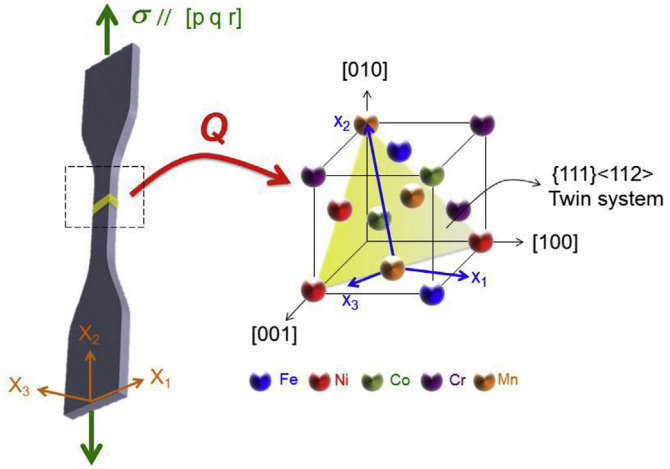


**Fig. C1.** Coordinate transformation of the stress from the sample frame to the twin frame for a single crystal orientated along [p q r] loading direction. The twin plane is shown by the yellow shaded area. The term [**Q**] is the transformation matrix.

**Table C1**
The fitting parameters $(a_1, a_2, a_3, a_4, \tau^{*}_{cr})$ of the generalized yield criterion Eq. (C.3) for the twin migration stress.

| $a_1$ | $a_2$ | $a_3$ | $a_4$ | $\tau^{*}_{cr}/C_{44}$ |
|---|---|---|---|---|
| 0.10 | 0.16 | 0.11 | −0.08 | 0.0043 |

The finite values of $a_1$,$a_2$,$a_3$, $a_4$ indicate that not only the glide shear stress, but also the other deviatoric stress components play a decisive role on the twin migration. Fig. C2 shows the yield surfaces for $\tau^{M}_{crit}$ constructed via utilizing Eq. (1) and the conventional Schmid Law in the principal stress space of $\sigma_1 - \sigma_2 - \sigma_3$. Most distinguishingly, the generalized yield criterion of the latent twin migration depicted by Eq. (1) exhibits strong asymmetric behavior unlike the six-fold symmetric plot based on the Schmid law. It is to be noted that the difference between the maximum stress differential between the Schmid law and the generalized yield criterion reaches almost a magnitude of 350 MPa, which is noteworthy. Meanwhile, the non-glide stresses contribute to this asymmetric twin migration behavior in FeNiCoCrMn alloy, the effect of the intrinsic asymmetry on the GPFE surface cross-section along {111}<112> direction (reflected as the unidirectional nature of the twinning shear) should not be neglected.

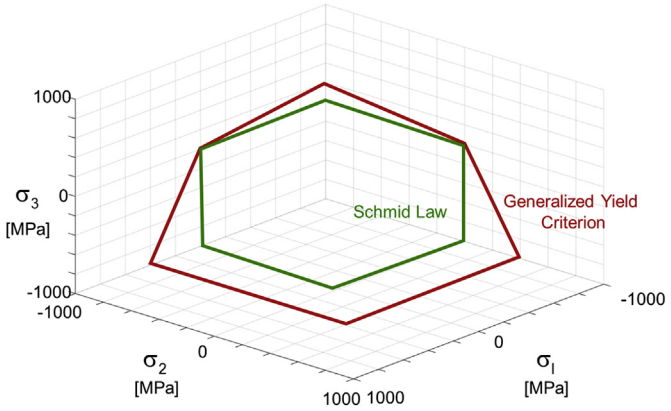


**Fig. C2.** The yield surface of the generalized yield criterion based on Eq. (C.3) and the conventional Schmid law in which the flow is dictated by the glide shear stress solely.

## References


[1] B. Cantor, I.T.H. Chang, P. Knight, A.J.B. Vincent, Microstructural development in equiatomic multicomponent alloys, Mater. Sci. Eng. A. 375–377 (2004) 213–218.
[2] F. Otto, A. Dlouhý, C. Somsen, H. Bei, G. Eggeler, E.P. George, The influences of temperature and microstructure on the tensile properties of a CoCrFeMnNi high-entropy alloy, Acta Mater. 61 (2013) 5743–5755.
[3] B. Gludovatz, A. Hohenwarter, D. Catoor, E.H. Chang, E.P. George, R.O. Ritchie, A fracture-resistant high-entropy alloy for cryogenic applications, Science 345 (2014) 1153–1158.
[4] W. Abuzaid, H. Sehitoglu, Critical resolved shear stress for slip and twin nucleation in single crystalline FeNiCoCrMn high entropy alloy, Mater. Char. 129 (2017) 288–299.
[5] P.P. Bhattacharjee, G.D. Sathiaraj, M. Zaid, J.R. Gatti, C. Lee, C.-W. Tsai, J.-W. Yeh, Microstructure and texture evolution during annealing of equiatomic CoCrFeMnNi high-entropy alloy, J. Alloy. Comp. 587 (2014) 544–552.
[6] M.C. Gao, J.-W. Yeh, P.K. Liaw, Y. Zhang, High-entropy Alloys: Fundamentals and Applications, Springer, 2016.
[7] G. Laplanche, A. Kostka, O.M. Horst, G. Eggeler, E.P. George, Microstructure evolution and critical stress for twinning in the CrMnFeCoNi high-entropy alloy, Acta Mater. 118 (2016) 152–163.
[8] Z.P. Lu, H. Wang, M.W. Chen, I. Baker, J.W. Yeh, C.T. Liu, T.G. Nieh, An assessment on the future development of high-entropy alloys: summary from a recent workshop, Intermetallics 66 (2015) 67–76.
[9] P. Chowdhury, D. Canadinc, H. Sehitoglu, On deformation behavior of Fe-Mn based structural alloys, Mater. Sci. Eng. R Rep. 122 (2017) 1–28.
[10] Y. Deng, C.C. Tasan, K.G. Pradeep, H. Springer, A. Kostka, D. Raabe, Design of a twinning-induced plasticity high entropy alloy, Acta Mater. 94 (2015) 124–133.
[11] I. Karaman, H. Sehitoglu, K. Gall, Y.I. Chumlyakov, H.J. Maier, Deformation of single crystal Hadfield steel by twinning and slip, Acta Mater. 48 (2000) 1345–1359.
[12] I. Karaman, H. Sehitoglu, A.J. Beaudoin, Y.I. Chumlyakov, H.J. Maier, C.N. Tome, Modeling the deformation behavior of Hadfield steel single and polycrystals due to twinning and slip, Acta Mater. 48 (2000) 2031–2047.
[13] K.S. Havner, A.H. Shalaby, A simple mathematical theory of finite distortional latent hardening in single crystals, in: Proceedings of the Royal Society of London a: Mathematical, Physical and Engineering Sciences, vol. 358, The Royal Society, 1977, pp. p.47–70.
[14] K.S. Havner, G.S. Baker, R.F. Vause, Theoretical latent hardening in crystals—I. General equations for tension and compression with application to fcc crystals in tension, J. Mech. Phys. Solid. 27 (1979) 33–50.
[15] P. Franciosi, M. Berveiller, A. Zaoui, Latent hardening in copper and aluminium single crystals, Acta Metall. 28 (1980) 273–283.
[16] P. Franciosi, A. Zaoui, Multislip in fcc crystals a theoretical approach compared with experimental data, Acta Metall. 30 (1982) 1627–1637.
[17] Latent Kocks, Hardening + secondary slip in aluminum+silver, Trans. Metall. Soci. AIME. 230 (1964), 1160-&.
[18] P.J. Jackson, Z.S. Basinski, Latent hardening and the flow stress in copper single crystals, Can. J. Phys. 45 (1967) 707–735.
[19] J.L. Bassani, T.-Y. Wu, Latent hardening in single crystals II. Analytical characterization and predictions, in: Proceedings of the Royal Society of London a: Mathematical, Physical and Engineering Sciences, vol. 435, The Royal Society, 1991, pp. p.21–41.
[20] R. Hill, Generalized constitutive relations for incremental deformation of metal crystals by multislip, J. Mech. Phys. Solid. 14 (1966) 95–102.
[21] H. Qiao, M.R. Barnett, P.D. Wu, Modeling of twin formation, propagation and growth in a Mg single crystal based on crystal plasticity finite element method, Int. J. Plast. 86 (2016) 70–92.

[22] M. Barnett, M. Setty, F. Siska, Estimating critical stresses required for twin growth in a magnesium alloy, Metall. Mater. Trans. A. 44 (2013) 2962–2969.
[23] T. Ezaz, M.D. Sangid, H. Sehitoglu, Energy barriers associated with slip–twin interactions, Phil. Mag. 91 (2011) 1464–1488.
[24] A. Ojha, H. Sehitoglu, L. Patriarca, H.J. Maier, Twin migration in Fe-based bcc crystals: theory and experiments, Phil. Mag. 94 (2014) 1816–1840.
[25] T.-Y. Wu, J.L. Bassani, C. Laird, Latent hardening in single crystals I. Theory and experiments, in: Proceedings of the Royal Society of London. Series a: Mathematical and Physical Sciences, vol. 435, 1991, pp. 1–19.
[26] D. Kuhlmann-Wilsdorf, Theory of plastic deformation: - properties of low energy dislocation structures, Mater. Sci. Eng. A. 113 (1989) 1–41.
[27] P. Franciosi, The concepts of latent hardening and strain hardening in metallic single crystals, Acta Metall. 33 (1985) 1601–1612.
[28] H. Suzuki, Segregation of solute atoms to stacking faults, J. Phys. Soc. Jpn. 17 (1962) 322–325.
[29] A. Ojha, H. Sehitoglu, Twinning stress prediction in bcc metals and alloys, Phil. Mag. Lett. 94 (2014) 647–657.
[30] A. Ojha, H. Sehitoglu, L. Patriarca, H.J. Maier, Twin nucleation in Fe-based bcc alloys—modeling and experiments, Model. Simulat. Mater. Sci. Eng. 22 (2014) 075010.
[31] G. Kresse, J. Furthmüller, Efficient iterative schemes for ab initio total-energy calculations using a plane-wave basis set, Phys. Rev. B 54 (1996) 11169–11186.
[32] G. Kresse, J. Hafner, Ab initio, Phys. Rev. B 48 (1993) 13115–13118.
[33] H.J. Monkhorst, J.D. Pack, Special points for Brillouin-zone integrations, Phys. Rev. B 13 (1976) 5188–5192.
[34] P.B. Chowdhury, H. Sehitoglu, R.G. Rateick, Predicting fatigue resistance of nano-twinned materials: Part I – role of cyclic slip irreversibility and Peierls stress, Int. J. Fatig. 68 (2014) 277–291.
[35] J.P. Hirth, J. Lothe, Theory of Dislocations, Krieger Publishing Company, 1982.
[36] S. Ogata, J. Li, S. Yip, Ideal pure shear strength of aluminum and copper, Science 298 (2002) 807.
[37] J. Wang, H. Sehitoglu, Twinning stress in shape memory alloys: theory and experiments, Acta Mater. 61 (2013) 6790–6801.
[38] S. Kibey, J.B. Liu, D.D. Johnson, H. Sehitoglu, Predicting twinning stress in fcc metals: linking twin-energy pathways to twin nucleation, Acta Mater. 55 (2007) 6843–6851.
[39] M.D. Sangid, T. Ezaz, H. Sehitoglu, Energetics of residual dislocations associated with slip–twin and slip–GBs interactions, Mater. Sci. Eng. A 542 (2012) 21–30.
[40] P. Chowdhury, H. Sehitoglu, Mechanisms of fatigue crack growth—a critical digest of theoretical developments, Fatig. Fract. Eng. Mater. Struct. 39 (2016) 652–674.
[41] S. Alkan, P. Chowdhury, H. Sehitoglu, R.G. Rateick, H.J. Maier, Role of nano-twins on fatigue crack growth resistance—experiments and theory, Int. J. Fatig. 84 (2016) 28–39.
[42] A. Ojha, L. Patriarca, H. Sehitoglu, Pseudoelasticity in Fe3Ga with boron-A combined atomistic–micromechanical treatment, Int. J. Plast. 72 (2015) 185–199.
[43] A.W. Cochardt, G. Schoek, H. Wiedersich, Interaction between dislocations and interstitial atoms in body-centered cubic metals, Acta Metall. 3 (1955) 533–537.
[44] I. Kireeva, Y. Chumlyakov, Z. Pobedennaya, D. Kuksgauzen, I. Karaman, H. Sehitoglu, Mechanisms of plastic deformation in [1$\bar{1}$1] -oriented single crystals of FeNiMnCrCo high entropy alloy, in: AIP Conference Proceedings, vol. 1783, AIP Publishing, 2016, p. p.020090.
[45] I.V. Kireeva, Y.I. Chumlyakov, Z.V. Pobedennaya, Y.N. Platonova, I.V. Kuksgauzen, D.A. Kuksgauzen, V.V. Poklonov, I. Karaman, H. Sehitoglu, Slip and twinning in the [ -149]-Oriented single crystals of a high-entropy alloy, Russ. Phys. J. 59 (2016) 1242–1250.
[46] K.S. Havner, Finite Plastic Deformation of Crystalline Solids, Cambridge University Press, 1992.
[47] A.H. Cottrell, The formation of immobile dislocations during slip, The London, Edinburgh, and Dublin Philosophical Magazine and Journal of Science 43 (1952) 645–647.
[48] J.P. Hirth, On dislocation interactions in the fcc lattice, J. Appl. Phys. 32 (1961) 700–706.
[49] Y.T. Zhu, X.L. Wu, X.Z. Liao, J. Narayan, L.J. Kecskés, S.N. Mathaudhu, Dislocation–twin interactions in nanocrystalline fcc metals, Acta Mater. 59 (2011) 812–821.
[50] R. Asaro, V. Lubarda, Mechanics of Solids and Materials, Cambridge University Press, 2006.
[51] M. Ardeljan, R.J. Mccabe, I.J. Beyerlein, M. Knezevic, Explicit incorporation of deformation twins into crystal plasticity finite element models, Comput. Meth. Appl. Mech. Eng. 295 (2015) 396–413.
[52] S.R. Kalidindi, Incorporation of deformation twinning in crystal plasticity models, J. Mech. Phys. Solid. 46 (1998) 267–290.
[53] R.A. Lebensohn, C.N. Tomé, A self-consistent anisotropic approach for the simulation of plastic deformation and texture development of polycrystals: application to zirconium alloys, Acta Metall. Mater. 41 (1993) 2611–2624.
[54] M. Knezevic, R.J. Mccabe, R.A. Lebensohn, C.N. Tomé, C. Liu, M.L. Lovato, B. Mihaila, Integration of self-consistent polycrystal plasticity with dislocation density based hardening laws within an implicit finite element framework: application to low-symmetry metals, J. Mech. Phys. Solid. 61 (2013) 2034–2046.
[55] F. Otto, N.L. Hanold, E.P. George, Microstructural evolution after thermomechanical processing in an equiatomic, single-phase CoCrFeMnNi high-entropy alloy with special focus on twin boundaries, Intermetallics 54 (2014) 39–48.
[56] E.J. Pickering, N.G. Jones, High-entropy alloys: a critical assessment of their founding principles and future prospects, Int. Mater. Rev. 61 (2016) 183–202.
[57] F. Otto, Y. Yang, H. Bei, E.P. George, Relative effects of enthalpy and entropy on the phase stability of equiatomic high-entropy alloys, Acta Mater. 61 (2013) 2628–2638.
[58] R.L. Fleischer, Substitutional solution hardening, Acta Metall. 11 (1963) 203–209.
[59] H. Neuhäuser, Mechanical properties of solid solutions and related topics, in: J. Lépinoux, D. Mazière, V. Pontikis, G. Saada (Eds.), Multiscale Phenomena in Plasticity: from Experiments to Phenomenology, Modelling and Materials Engineering, Springer, Netherlands, Dordrecht, 2000, pp. 99–116.
[60] T. Mohri, H. Miyamoto, Y. Terada, T. Suzuki, Statistical thermodynamics of configurational hardening in a solid solution, Mater. Sci. Eng. A. 267 (1999) 151–158.
[61] W.M. Lomer, A dislocation reaction in the face-centred cubic lattice, the London, Edinburgh, and Dublin, Phil. Mag. J. Sci. 42 (1951) 1327–1331.
[62] L. Rémy, The interaction between slip and twinning systems and the influence of twinning on the mechanical behavior of fcc metals and alloys, Metall. Trans. A. 12 (1981) 387–408.
[63] S. Asgari, E. El-Danaf, S.R. Kalidindi, R.D. Doherty, Strain hardening regimes and microstructural evolution during large strain compression of low stacking fault energy fcc alloys that form deformation twins, Metall. Mater. Trans. A. 28 (1997) 1781–1795.
[64] A. Coujou, A. Beneteau, N. Clement, Observation in situ dans un met du cisaillement d'un joint de macle coherent Σ3 par une micromacle de deformation, Acta Metall. Mater. 40 (1992) 337–344.
[65] S. Alkan, H. Sehitoglu, Non-Schmid response of Fe3Al: the twin-antitwin slip asymmetry and non-glide shear stress effects, Acta Mater. 125 (2017) 550–566.
[66] L. Capolungo, I.J. Beyerlein, C.N. Tomé, Slip-assisted twin growth in hexagonal close-packed metals, Scripta Mater. 60 (2009) 32–35.
[67] I.J. Beyerlein, L. Capolungo, P.E. Marshall, R.J. Mccabe, C.N. Tomé, Statistical analyses of deformation twinning in magnesium, Phil. Mag. 90 (2010) 2161–2190.
[68] S. Mahajan, G.Y. Chin, Formation of deformation twins in fcc crystals, Acta Metall. 21 (1973) 1353–1363.
[69] A.J.E. Foreman, Dislocation energies in anisotropic crystals, Acta Metall. 3 (1955) 322–330.
[70] Y. Wu, A. Ojha, L. Patriarca, H. Sehitoglu, Fatigue crack growth fundamentals in shape memory alloys, Shape Mem. Superelasticity. 1 (2015) 18–40.
[71] E.B. Tadmor, R.E. Miller, Modeling Materials: Continuum, Atomistic and Multiscale Techniques, Cambridge University Press, 2011.
[72] Z. Jin, T.R. Bieler, An in-situ observation of mechanical twin nucleation and propagation in TiAl, Philos. Mag. A 71 (1995) 925–947.
[73] P. Müllner, A.E. Romanov, Internal twinning in deformation twinning, Acta Mater. 48 (2000) 2323–2337.
[74] J.W. Christian, S. Mahajan, Deformation twinning, Prog. Mater. Sci. 39 (1995) 1–157.
[75] U.F. Kocks, Latent hardening and secondary slip in aluminum and silver, Trans. Metall. Soc. AIME. 230 (1964) 1160–1167.
[76] R.J. Asaro, Micromechanics of crystals and polycrystals, Adv. Appl. Mech. 23 (1983) 1–115.